OMV AUSTRALIA PTY LTD
ACN 082 932 027

SOLE DEVELOPMENT
(Patricia Baleen Extension)

Petrophysical Review

SD-01-RE-0012
Part B

March 2004

Table of Contents

1 INTRODUCTION 2

2 CORE DATA 2

2.1 Rock Samples Recovered 2
2.1.1 Conventional Core 2
2.1.2 Sidewall Samples 3
2.2 Grain Density 3
2.3 In-Situ Stress Transforms 4
2.4 Porosity vs. Permeability 5
2.5 Vertical Permeability 9
2.6 Probe Permeameter 10
2.7 Clay Conductivity 11
2.8 Cementation Exponent 12
2.9 Saturation Exponent 12
2.10 Irreducible Water Saturation 13
2.11 Capillary Pressures 15
2.12 Residual Gas Saturations 20
2.13 Relative Permeability 21

3 PETROPHYSICAL EVALUATION 22

3.1 Normalisation 22
3.2 Temperature 23
3.3 Porosity 24
3.4 Permeability 25
3.5 True Formation Resistivity 25
3.6 Formation Water Resistivity 25
3.7 Hydrocarbon Saturation from Logs 26
3.8 Net Sands 26

4 INDIVIDUAL WELLS 27

4.1 Sole-2 27
4.2 Sole-1 28
4.3 Hammerhead-1 28
4.4 Leatherjacket-1 28
4.5 Dart-1 29

5 DISCUSSION 29

5.1 Porosity 29
5.2 Permeability 31
5.3 Differences with Previous Evaluations 33
5.4 Water Saturations 34
5.4.1 Resistivity in Sole-2 Washouts 34
5.4.2 Saturation-Height Model Comparison 35
5.5 Representative Sampling 37
5.6 Formation Water Salinity 38
5.7 Pressure Regimes 41
5.8 Reservoir Quality and Water Saturation 43
5.9 Uncertainty 44

6 CONCLUSIONS 46

7 RECOMMENDATIONS 46

Appendices

BA Saturation-Height Function Implementation.
BB Log Name Convention For Sole Field Study.
BC Log Evaluation Summary & Plots.

Figures

B1a. Grain density variation with porosity for Sole-2.

B1b. Histogram of grain density data from Sole-2.

B2. In-situ and ambient measurements of porosity are compared.

B3. In-situ and ambient measurements of permeability are compared.

B4a. Ambient air permeability vs. porosity for Sole-2.

B4b. Stressed air permeability vs. porosity for Sole-2.

B4c. In-situ permeability vs. porosity for Sole-2.

B4d. In-situ permeability vs. porosity for Sole-2, samples coded by GR.

B4e. In-situ measured vs. estimated permeability for Sole-2.

B4f. Histogram of the differences between estimated & measured permeabilities for Sole-2.

B4g. In-situ permeability vs. porosity for Sole-2, samples coded by GR with estimates overlayed.

B5a. Vertical and horizontal permeabilities are compared for Sole-2.

B5b. Porosities for horizontal and vertical plugs are compared for Sole-2.

B6a. Calibration of mini-permeameter data to core plugs for Sole-2.

B6b. Check of calibrated mini-permeameter data to core plugs.

B7. Clay conductivity vs. in-situ core porosity for Sole-2.

B8. Archie and Waxman-Smits cementation exponents vs. porosity.

B9a. Archie resistivity index vs. porosity.

B9b. Waxman-Smits resistivity index vs. porosity.

B10a. Irreducible water saturation vs. porosity.

B10b. Irreducible water saturation vs. permeability.

B11a. Air-brine capillary pressure curves for high GR Facies in Sole-2 using porosity in legend.

B11b. Air-brine capillary pressure curves for low GR Facies in Sole-2 using porosity in legend.

B11c. Average capillary pressure curves for Sole-2 are compared with the measured data.

B11d. Air-brine capillary pressure curves for high GR Facies in Sole-2 using permeability in legend.

B11e. Air-brine capillary pressure curves for low GR Facies in Sole-2 using permeability in legend.

B11f. Respresentative capillary pressure curves for high GR Facies in Sole-2 are compared with their Facies and permeability based saturation-height function equivalents.

B11g. Respresentative capillary pressure curves for low GR Facies in Sole-2 are compared with their Facies and permeability based saturation-height function equivalents.

B11h. Respresentative capillary pressure curves for all Facies in Sole-2 are compared with their permeability based saturation-height function equivalents.

B12. Residual gas saturation data from core experiments for Sole-2.

B13a. In-situ gas permeability at irreducible water saturation vs. in-situ permeability for Sole-2.

B13b. In-situ water permeability at residual gas saturation vs. in-situ permeability for Sole-2.

B14a. Before and after GR normalisation in Sole-1.

B14b. Before and after GR normalisation in Hammerhead-1.

B14c. Before and after GR normalisation in Leatherjacket-1.

B14d. Before and after GR normalisation in Dart-1.

B15a. Derivation of sonic porosity relationship in Sole-2 & Dart-1.

B15b. Derivation of porosity from GR based on core porosities.

B16. Histogram of apparent formation water salinity for water-leg in Sole-2.

B17a. The effect of lithology cut-off on net-to-gross in Sole-1.

B17b. The effect of lithology cut-off on net-to-gross in Sole-2.

B18a. Porosity from core vs. porosity from log evaluation for Sole-2.

B18b. Histogram of the differences between log & core porosities.

B18c. Differences between log & core porosities vs. depth in Sole-2.

B18d. UV & white light photos of 805.85-806.35 m RT.

B18e. Histogram of the differences between recalibrated log & core porosities.

B19a. Permeability from core vs. that from logs for Sole-2.

B19b. Histogram of differences between log & core permeabilities.

B19c. Differences between log & core permeabilities vs. depth.

B20. Actual and modelled resistivities 837-847 m RT in Sole-2.

B21a. Log & SHF based gas saturations are shown for Sole-1.

B21b. Log & SHF based gas saturations are shown for Sole-2.

B22a. Log & SHF based gas saturations are compared for Sole-1 & 2.

B22b. Histogram of Log-SHF gas saturations for Sole-1 & 2.

B23a. Normalised histogram of porosities for Sole-1 & 2.

B23b. Normalised histogram of permeabilities for Sole-1 & 2.

B24a. Formation water salinity variation with depth in Sole Field.

B24b. Histogram of apparent formation water salinity near FWL in Sole Field.

B24c. Histogram of apparent formation water salinity away from FWL in Sole Field.

B24d. Histogram of apparent formation water salinity for all zones in Sole-1, 2 & Dart-1.

B24e. Variation of apparent formation water salinity in Latrobe away from Sole Field.

B25a. Available pressure data is plotted for the Sole Field.

B25b. Pressure data for all the study wells is combined.

B26a. Hydrocarbon saturation vs. porosity for the Sole area.

B26b. Hydrocarbon saturation vs. permeability for the Sole area.

B27a. Uncertainty ranking for components making up porosity.

B27b. Uncertainty ranking for components making up hydrocarbon saturations.

Tables

B1. Summary of coring operations and core recovered in Sole-2.

B2. Log normalisations carried out during the course of this study

B3. Comparisons between earlier petrophysical evaluations and the work reported herein for Sole-1 and Sole-2.

B4a. Input parameters for Monte-Carlo porosity modelling in Sole Field.

B4b. Parameters for Monte-Carlo water saturation modelling in Sole.

SUMMARY

Following the drilling of the Sole-1 and Sole-2 gas discovery wells, all the available Petrophysical data for the area has been incorporated into a Petrophysical Review of the Sole accumulation. The reservoir properties derived will be carried forward into reservoir modelling for volumetric determinations and field development planning.

The main points highlighted by the Petrophysical review are:

- Sole-2 core data has been used to construct: ambient to in-situ porosity and permeability transforms, porosity to permeability transforms, cementation and saturation exponents, saturation-height functions, residual gas saturation relations and in-situ fluid permeabilities.
- For the Sole Gas Field, porosities should be calculated based on the density log with a gas correction using the invaded zone resistivity log to correct for the fluid density in the invaded zone.
- In Sole-2, differences between core and log porosities in the washed out hole section are thought to be due to excess mud invasion into the permeable sands causing increased density measurements. A correction has been applied to the density porosities to improve the match with the core data. The uncertainty addressed by such a model has been quantified.
- In Sole-2, permeabilities estimated from logs compare reasonably with those measured on core. The technique requires normalisation of the gamma ray log in other wells to match that in Sole-2 over selected intervals for application in other Upper Latrobe penetrations. Significant uncertainty in absolute permeability values remains.
- Formation water salinity in the Upper Latrobe Sands of the Sole Field is thought to be in the range from 26,000 to 40,000 ppm NaCl equivalent. Use of 33,000 ppm NaCl eq. for petrophysical evaluation is recommended.
- Gas saturations from capillary pressure based saturation-height functions compare well with log derived water saturations, although there are some differences in the transition zones of Sole-1 and Sole-2. These are thought to be due to limitations of the resistivity readings through these zones in each well.
- The GWC is located near 816.6 mss from Sole-2. Sole-1 gives a deeper GWC near 818.1 mss, however the GWC is thought to be common, with a most likely depth near 817 mss.

1 INTRODUCTION

Following the drilling of the Sole-2 gas appraisal well, the available Petrophysical data for Sole-1, Sole-2, Dart-1, Hammerhead-1 and Leatherjacket-1 have been incorporated into a Petrophysical Review of the Sole accumulation. The reservoir properties derived will be carried forward into reservoir modelling for volumetric determinations and field development planning.

In addition, this report forms a basis for future petrophysical evaluation in the permit area.

The report is laid out beginning with the basic data available for Petrophysical calibration, the appropriate log evaluation models to use and following on with specific information from individual wells. Finally, all the learning points are drawn together to form a basis for improved understanding of the Sole Field as a whole.

Given the small difference between the FWL and GWC of approximately 0.1m, the FWL and GWC were considered interchangeable in this report. This has an insignificant impact on the volumetric estimates.

2 CORE DATA

This section discusses the core data available and the laboratory analyses conducted to date.

2.1 Rock Samples Recovered

Samples suitable for petrophysical calibration purposes have been obtained in either of two ways: through conventional coring, or through sidewall coring. The latter samples are only suitable for grain density and mineralogical work.

2.1.1 Conventional Core

The only well in the study with core acquired in the Latrobe Sands is Sole-2. There were problems during the core acquisition resulting in poor recovery (OMV, 2002). Consequently, there is some uncertainty in positioning the cores. Cores 2 and 4, in particular can be located over a range of depths relative to the logs. The coring details are included as Table B1 (from OMV, 2002).

A suite of 1 ½" diameter horizontal plug samples was cut at a rate of every 30 to 50 cm for Routine Core Analysis (RCA). There were also 27 vertical plugs taken at approximately 1 metre intervals.

The Routine Core Analysis consisted of porosity, air permeability and grain density. Probe permeametry was conducted on 173 points. Surface Spectral Gamma Ray was run over the four cores. Additionally, 19 samples were analysed at multiple overburden pressures. Seven whole core sections were removed for possible later Special analysis.

Special core analyses have also been carried out on this core material, allowing calibration of petrophysical models. These results are discussed and analysed in the following sections.

Table B1 Summary of coring operations and core recovered in Sole-2

Core No.	Interval (m RT)	Metres Cut	Recovery (%)	Recovery (m)	Comments
1	773 to 791	18	78	14	
2	791 to 801	10	24.6	2.46	Barrel jammed after 10 m.
3	801 to 804.5	3.5	57.4	2.01	Barrel jammed after 3.5 m.
4	804.5 to 814.5	10	56.7	5.67	Barrel jammed after 10m.

2.1.2 Sidewall Samples

Sidewall samples were acquired in both Sole-1 and Sole-2. Only petrographic work has been carried out on these samples.

2.2 Grain Density

The grain density data from Sole-2 is displayed in Figure B1a as a function of in-situ porosity. This approach is used to determine if there are lithological components in the lower porosities with higher grain densities, as is common in some formations.
In Sole, there is no clear trend in the grain density data as a consequence of porosity, so use of an average grain density is recommended. Figure B1b shows a histogram of the available grain density data. The mean (P50) value of the grain density is 2.647 g/cc, while the P90 value is 2.620 and the P10 value 2.657 g/cc.

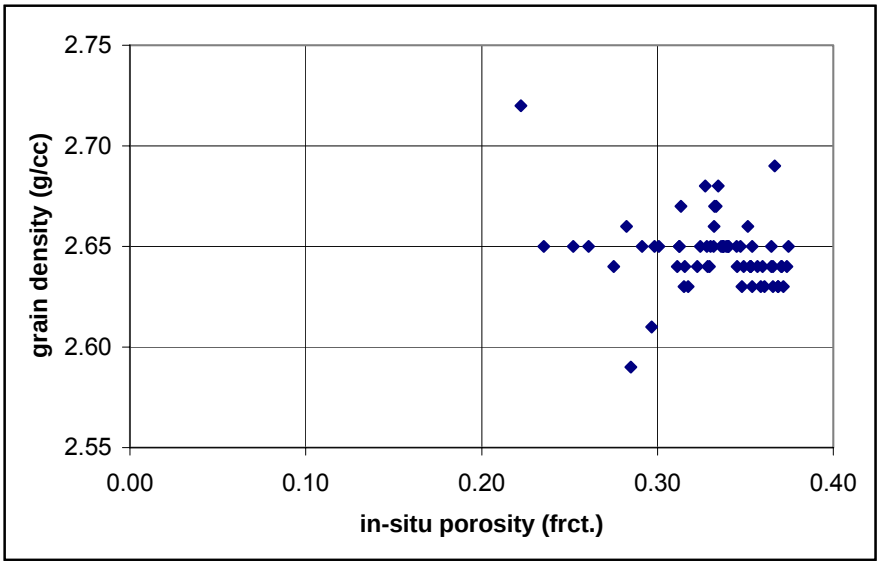

Figure B1a
The variation of grain density with porosity is examined for the Sole-2 core data.

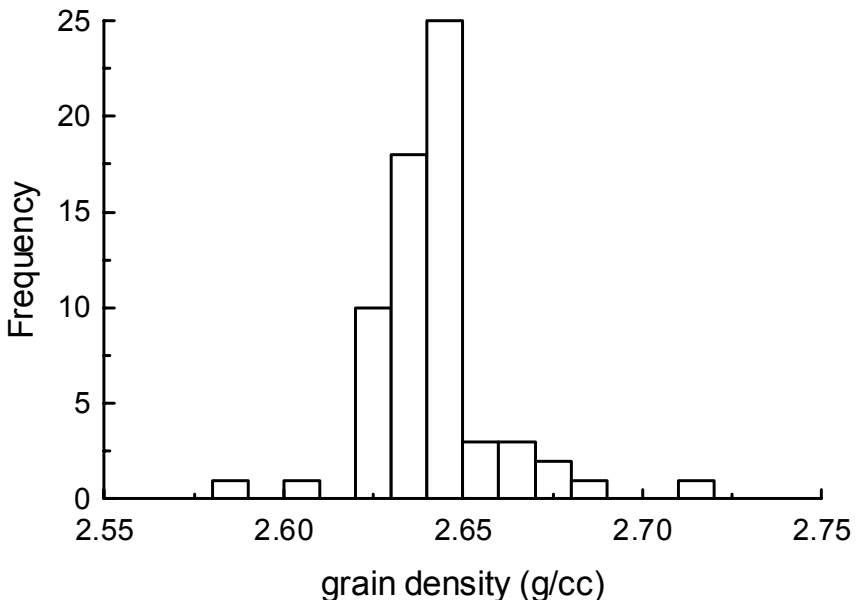

Figure B1b
A histogram of the grain density data from the Sole-2 core analyses.

2.3 In-Situ Stress Transforms

Figure B2 compares the porosities measured on core at isostatic net overburden stress (1049 psi using the formula of Nieto et. al. 1990) with those measured at laboratory conditions (400 psi). A straight line relationship has been fitted through the data, being:

$$\phi_{is} = 0.974\ \phi_{amb}$$

where ϕ_{amb} is the porosity at laboratory conditions and ϕ_{is} is the porosity at in-situ conditions, both expressed as a fraction of bulk volume.

This relationship is recommended for use when converting from laboratory measurements of ambient porosity to in-situ estimates of porosity.

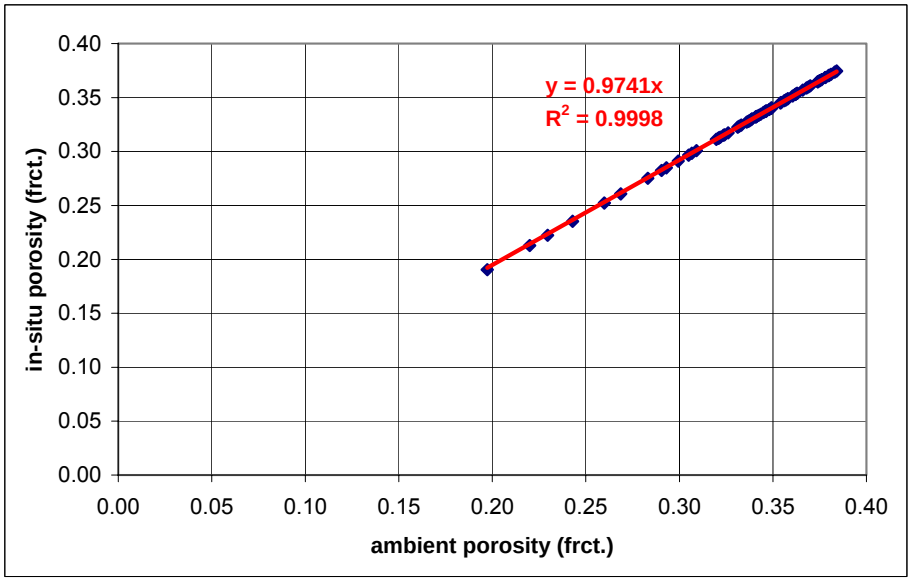

Figure B2
The relationship between in-situ and ambient measurements of core porosity is shown for the Sole-2 core analyses.

Figure B3 makes a similar comparison between permeabilities measured on core at isostatic net overburden stress (1049 psi) with those measured at laboratory conditions (400 psi). A relationship has also been fitted through this data, being:

$$k_{is} = 0.769\ k_{amb}^{1.017}$$

where k_{amb} is the permeability at ambient conditions and k_{is} is the air permeability at in-situ stress, both expressed in milliDarcies.

This relationship is recommended for use when converting from laboratory measurements of ambient air permeability to in-situ estimates of air permeability.

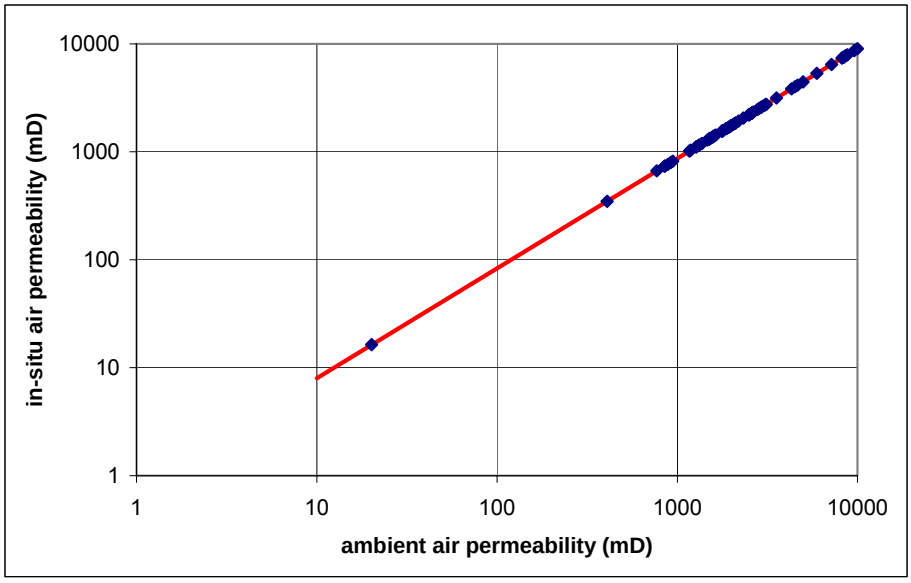

Figure B3
The relationship between in-situ and ambient measurements of core permeability is shown for the Sole-2 core analyses.

To use these permeability estimates as in-situ gas permeabilities still requires a correction from air permeabilities to gas permeabilities. Klinkenberg correction is thus necessary. In the absence of Klinkenberg measurements on the core samples, the approximation below is recommended:

$$K_{is} = a \cdot K_{stress,air}$$

where a = minimum of (1.0 or $0.9038 \cdot K_{stress,air}^{0.0086}$), $K_{stress,air}$ is the air permeability estimate and K_{is} is the Klinkenberg corrected permeability, both expressed in milliDarcies. Note this formula has been derived by the author for use during the course of his work.

2.4 Porosity vs. Permeability

All the porosity and permeability data available from Sole-2 are plotted in Figures B4a, b and c. The first figure shows the data measured at laboratory “ambient” conditions, the second at in-situ stress using air and the last Figure after correction to in-situ stress and fluids (§2.3).

In Figure B4a, b and c a small difference between the porosity to permeability relationships is seen between the routine and vertical plugs. The permeabilities of the vertical plugs are generally slightly less than those of their horizontal equivalents. The comparison is discussed in detail in the next section (§2.5).

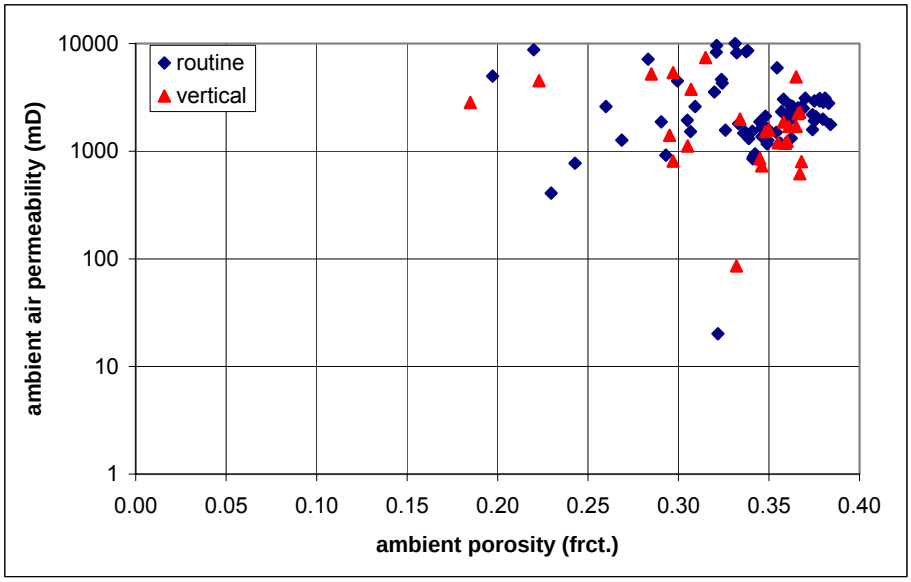

Figure B4a
Ambient porosity and air permeability data are shown for the Sole-2 core analyses.

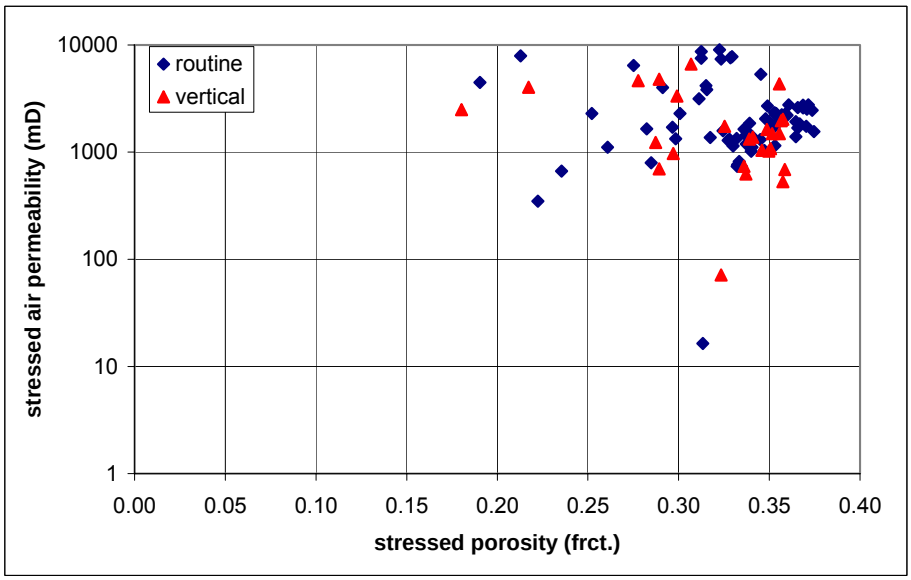

Figure B4b
The relationship between in-situ porosities and stressed air permeabilities is shown for the Sole-2 core analyses.

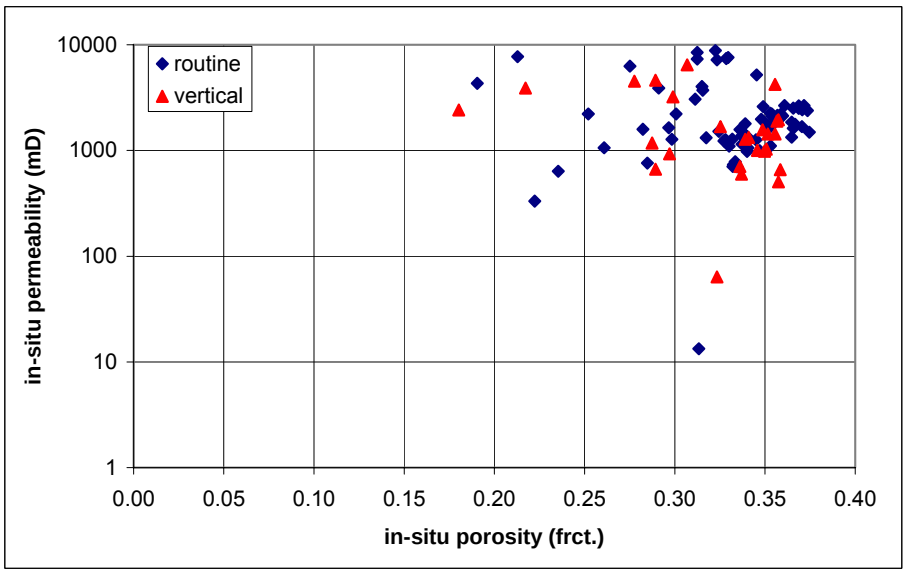

Figure B4c
The relationship between in-situ porosities and permeabilities is shown for the Sole-2 core analyses.

Attempts to construct a permeability transform using porosity alone were unsuccessful, yielding essentially horizontal lines with correlation coefficients of zero! Clearly, these porosity versus permeability plots show that there is another control on permeability in Sole rather than porosity alone. Baker (2003) suggests from Petrographic work that grain size and sorting are controls on permeability. He also highlights that gamma ray increases with decreasing grain size. Accordingly, the efficacy of a continuous gamma ray based permeability model has been investigated.

Using the depth-matched log data, it was possible to extract log gamma ray (GR) values for each of the core plug locations. This data was included with the in-situ core porosities and permeabilities in Figure B4d. The lower GR values have higher permeabilities at lower porosities, suggesting that the GR log can be used to guide porosity to permeability transforms.

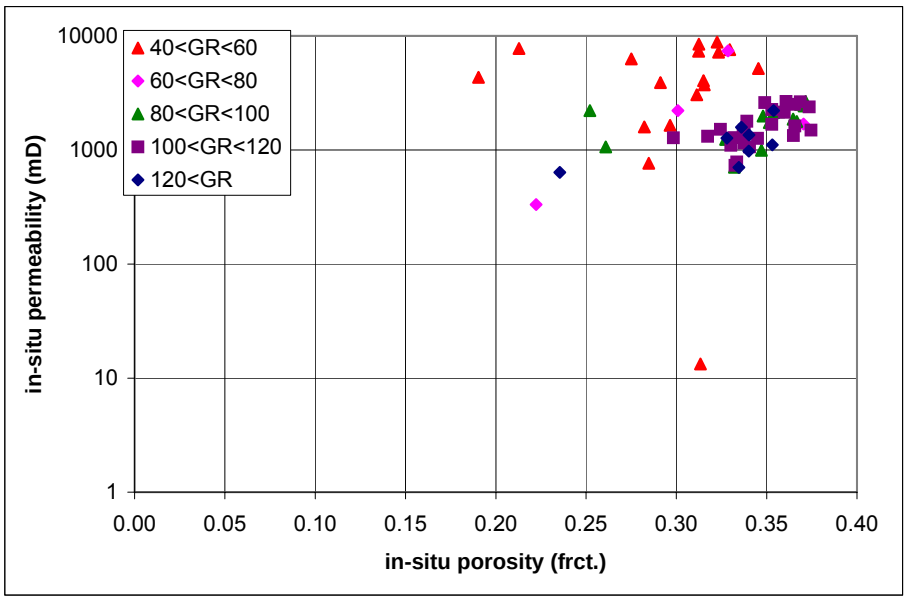

Figure B4d
The relationship between in-situ porosities and permeabilities is shown for the Sole-2 core analyses using a gamma ray based colour scheme.

Regression analysis using the model below yields Figure B4e comparing the modelled and measured permeabilities. Figure B4f shows a histogram of the differences, while the comparison with the measured data is shown as Figure B4g, as a porosity versus permeability diagram.

$$Vsh = (GR-GR0)/(GR1- GR0)$$

$$\phi_e = (1-Vsh)\cdot\phi_t$$

$$k_{is} = 10^{(a\cdot\phi e + b)}$$

where GR is the gamma ray value of the core plug with porosity ϕ_t (expressed as a fraction of bulk volume). GR_0 is the nominal gamma ray value of the cleanest sand, GR1 is the nominal GR value of the impermeable shales, while a and b are fitting parameters. For the model shown in *Figure B4e, B4f* and B4*g*, GR_0 = -4 , GR_1=177, a=7.29 and b=2.24 . Since the distribution is close to normally distributed, the uncertainty in permeability estimated can be derived using the “Student’s T” model, being $10^{0.50}$ at the P90/P10 levels i.e. a factor of 3.2.

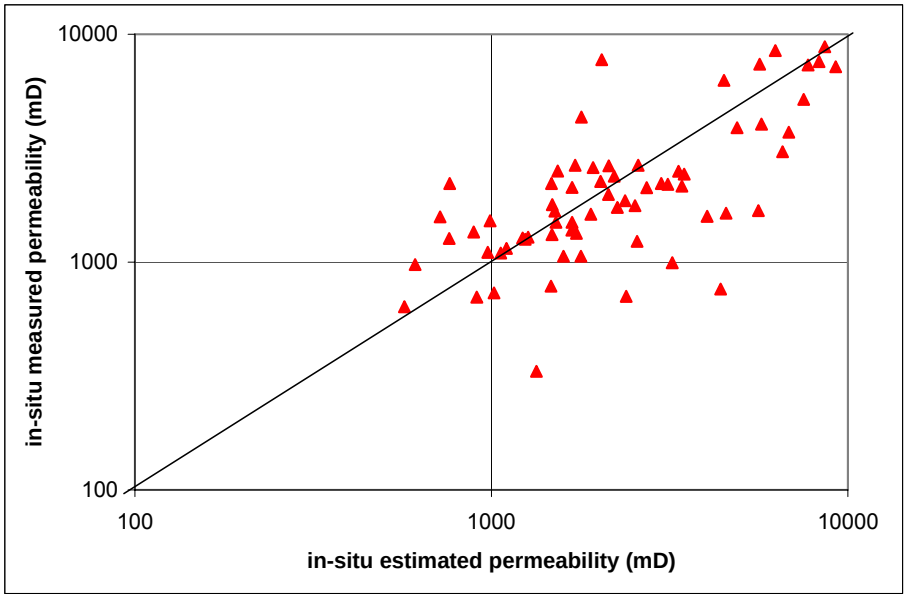

Figure B4e
The modelled and measured in-situ permeability estimates for Sole-2 core material are compared. The black line is the ideal relationship.

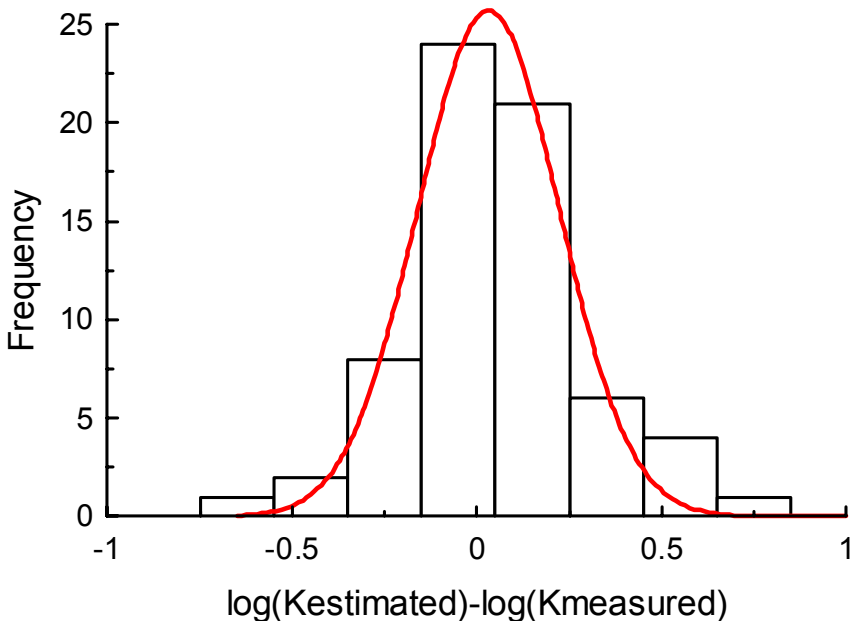

Figure B4f
The differences between the modelled and measured in-situ permeability estimates for Sole-2 core material are compared. The mean is close to zero, while the standard deviation is 0.39. The red line serves to show that the differences are close to normally distributed.

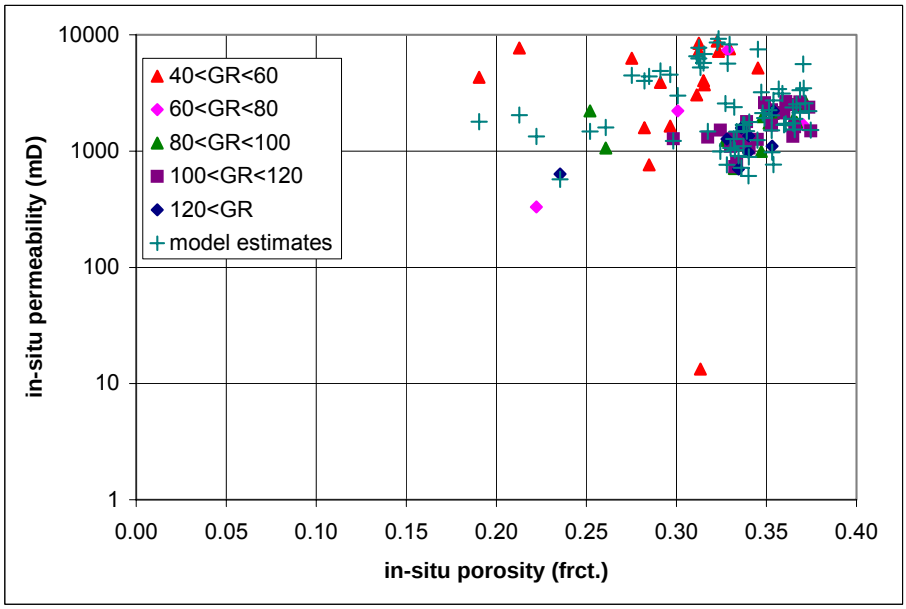

Figure B4g
The measured in-situ porosities and permeabilities for the Sole-2 core plugs are compared with estimates from GR based permeability modelling.

Note that this permeability model is similar to that used by Young et. al. 2002 for the Iona Field. Comparisons between this model and the log measurements will be made in §6.

It should also be remembered that to use this technique field-wide implies that GR log normalisation is required for all wells other the Sole-2. Other wells must match the Sole-2 GR log over those intervals expected to be similar.

2.5 Vertical Permeability

A number of plugs have been acquired in a vertical orientated through the Sole-2 core also. As discussed in the previous section, in general, there is a small difference between the porosity to permeability relationships for the routine and vertical plugs (Figure B4c). The permeabilities of the vertical plugs are generally slightly less than those of their horizontal equivalents from “twin” plugs (Figure B5a).

A direct comparison between the horizontal and vertical permeabilities of the “twin” plugs is made in Figure B5a. It is apparent that a Kv/Kh ratio of 0.75 can describe the variation within each sand unit.

Figure B5b Illustrates that the permeability differences are not due to the different porosities of the “twin” plugs.

When considering vertical permeability for reservoir modelling, the vertical permeability between layers with different horizontal permeabilities provides the strongest control on aquifer movement. Hence, barriers should be modelled in the reservoir simulator where permeability contrasts are significant such that one layer will flow preferentially over another.

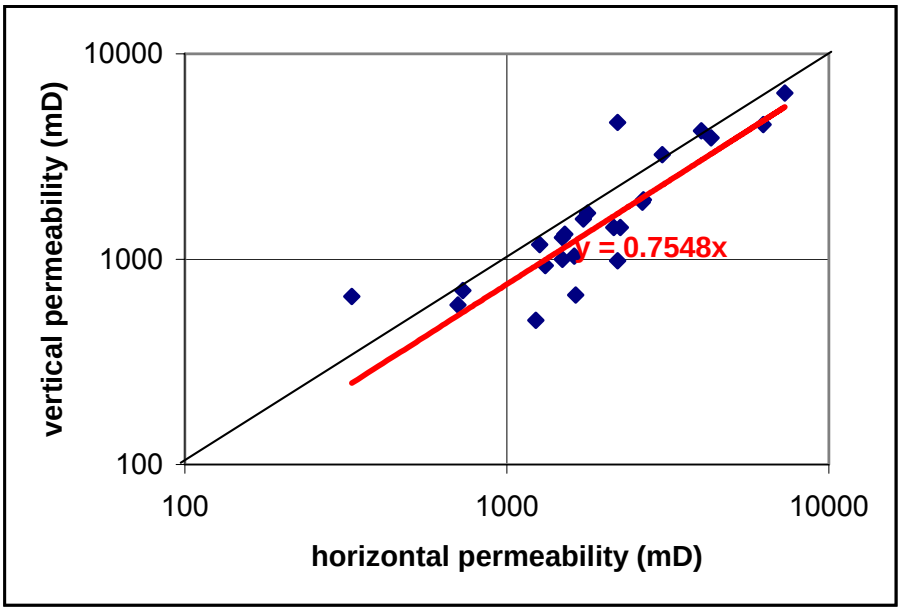

Figure B5a
The permeabilities for the horizontal and vertical “twin” plugs are compared. The best fit line suggests a Kv/Kh ratio of 0.75 is appropriate.

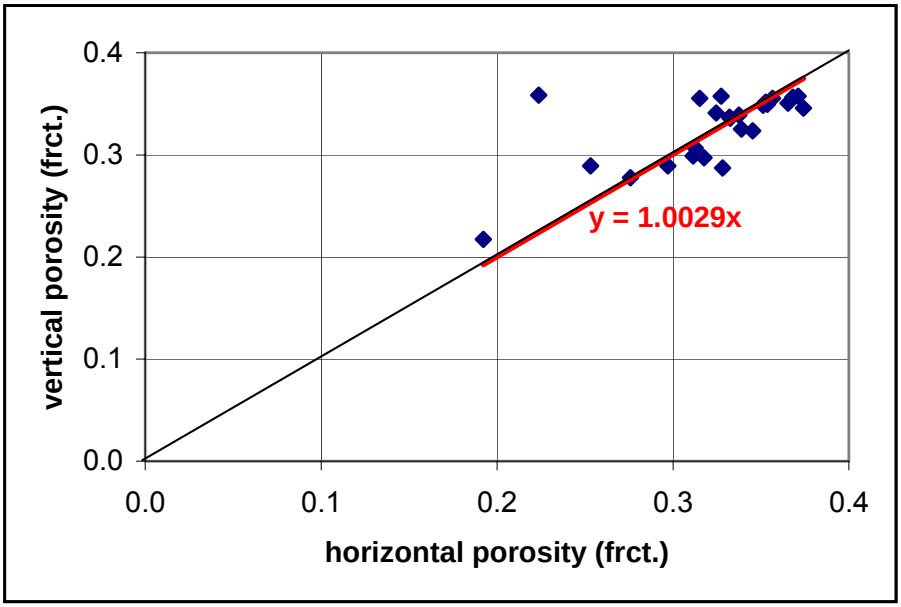

Figure B5b
The porosities for the horizontal and vertical "twin" plugs are compared. The best fit line has a slope close to 1.0, as hoped.

2.6 Probe Permeameter

Since a probe permeameter was also run over the Sole-2 core, this data has also been examined.

Initially the probe to core plug permeability was checked. Since the probe permeabilities are air permeabilities at ambient conditions, these are compared with the core plug measurements at similar depths in Figure B6a. It is clear that the probe permeabilities are generally lower than those measured on the routine core plugs. The red line shown is a best fit through the data, having the formula below:

$$K_{probe,cal} = 10^{(0.574 \cdot Kprobe + 1.591)}$$

where K_{probe} is the measured probe permeameter value while $K_{probe,cal}$ is the calibrated probe permeameter permeability at ambient conditions with air. *Figure B6b* shows the robustness of the calibration equation, comparing the re-calibrated probe permeabilities with those from the routine core plugs at similar depths.

For comparison with in-situ permeability estimates, the conversions discussed in §2.3 should be applied to the probe permeability measurements.

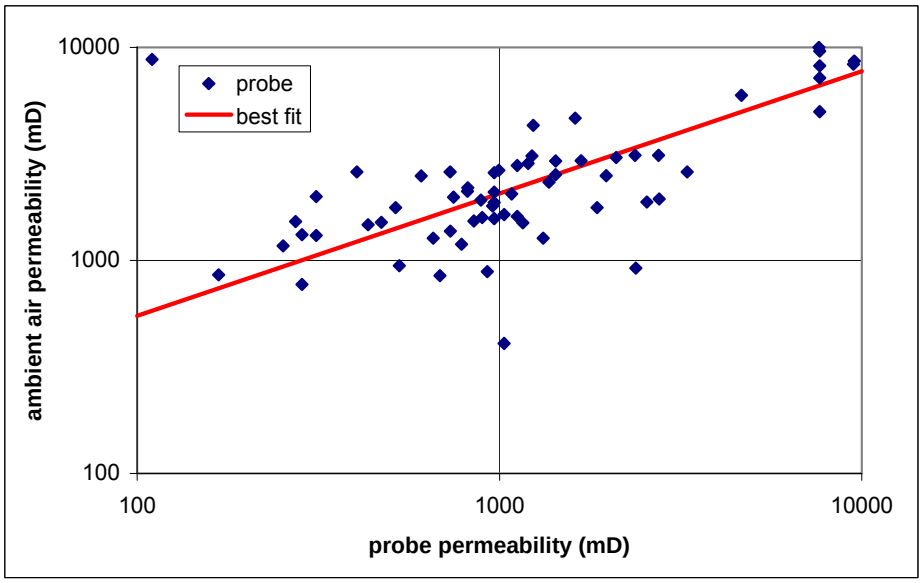

Figure B6a
The probe permeabilities are compared with ambient air permeabilities from the core plugs taken at similar depths.

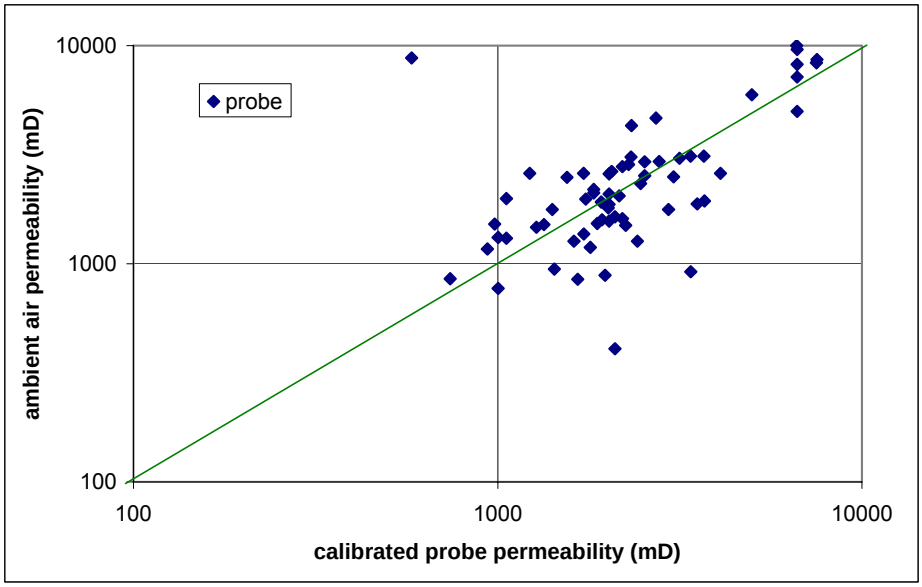

Figure B6b
The calibrated probe permeabilities are compared with ambient air permeabilities from the core plugs taken at similar depths.

2.7 Clay Conductivity

Clay conductivity has been measured using the multiple salinity (Hoyer-Spann) method on 12 samples from Sole-2. This experiment allows estimates of BQv to be made, from which clay conductivity (Qv) can be determined if assumptions are made about clay-bound water salinity and reservoir temperature to determine the factor B (Waxman & Smits, 1968). For the numbers shown clay-bound water salinity has been chosen as 35,000 ppm NaCl eq. and the temperature near 46 C. Fortunately, the calculation of B is relatively insensitive to the likely range of these values for Sole, so the impact on uncertainty in Qv is small compared to the uncertainty in the relationship derived by fitting through the data.

The Q_v relationship derived (*Figure B7*) was:

$$Q_v = 0.105/\phi - 0.13,$$

where ϕ is the (total) porosity expressed as a fraction of pore volume. The function has a minimum value of 0.0 and a maximum Q_v of 1.0. The uncertainty at the P10/P90 level is ±57%, shown as the red and blue lines respectively on *Figure B7*.

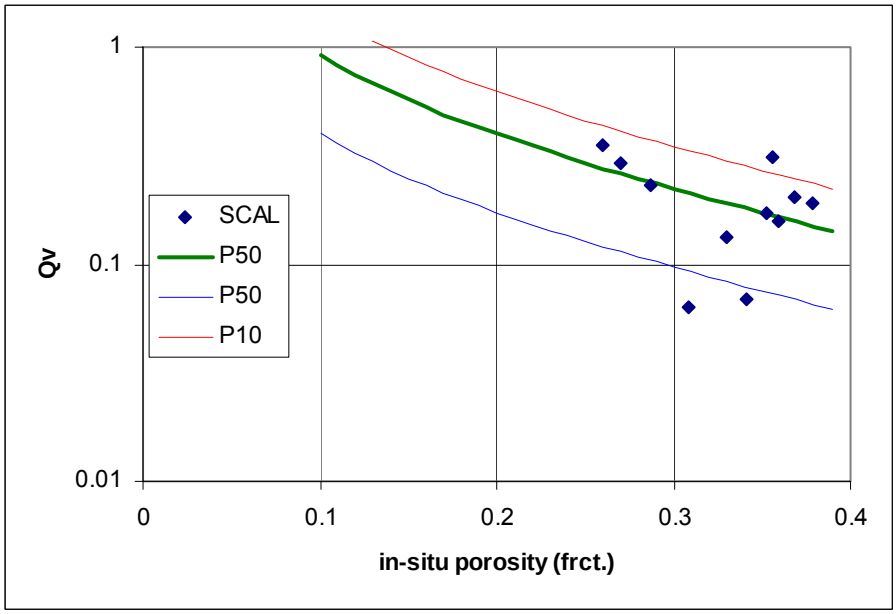

Figure B7
The clay conductivity values determined using the multiple salinity technique are plotted against in-situ core porosity.

2.8 Cementation Exponent

Formation Resistivity Factor experiments have been carried out on 12 samples from Sole-2. Figure B8 shows the cementation exponents for the Archie and Waxman-Smits (from Hoyer-Spann multiple salinity experiments) equations. There are no meaningful relationships between either the Archie exponent "m" or the Waxman-Smits "m*" and porosity. Hence, average values for these numbers are recommended. Uncertainty estimates have been derived assuming a normal distribution. These numbers are:

Archie equation: m = 1.74 ± 0.07

Waxman-Smits equation: m* = 1.85 ± 0.05

Note that the uncertainty values quoted are at the P90/P10 levels.

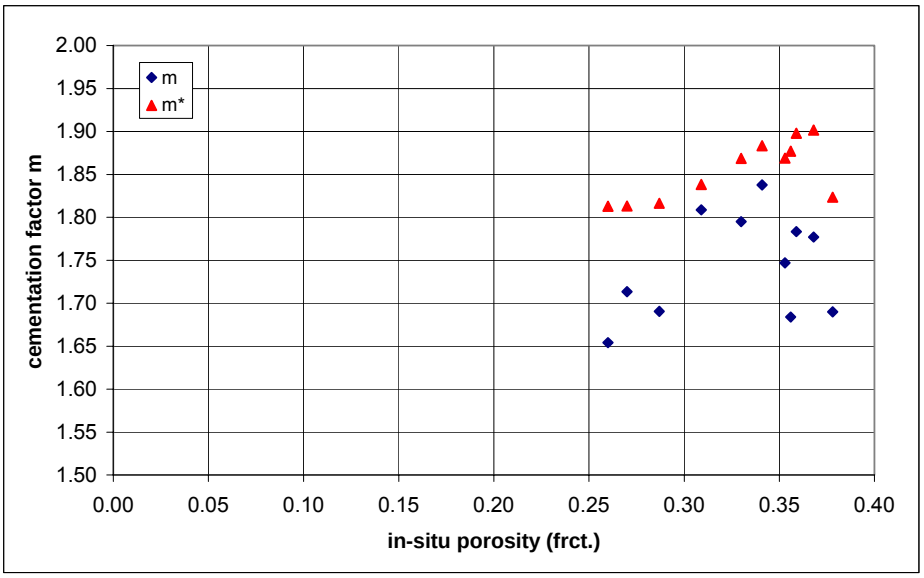

Figure B8
The Archie (m) and Waxman-Smits (m) cementation exponents are plotted as a function of porosity, looking for meaningful relationships.*

2.9 Saturation Exponent

Resistivity Index experiments were carried out on 12 samples from Sole-2. Figure B9a shows the results for the Archie equation. The most likely value for the saturation exponent "n" is 1.93, while the P90 and P10 values are 2.09 and 1.77 respectively – based on a normal distribution. Note that for this derivation, the data from the pyritic sample 58B has been excluded. This sample had anomalously low saturation exponents (less than 1.0).

Figure 9b shows similar results for the Waxman-Smits equation. The most likely value for the saturation exponent "n*" is now 2.19, while the P90 and P10 values are 1.99 and 2.39 respectively. Note that for this derivation too, the data from the pyritic sample 58B has been excluded.

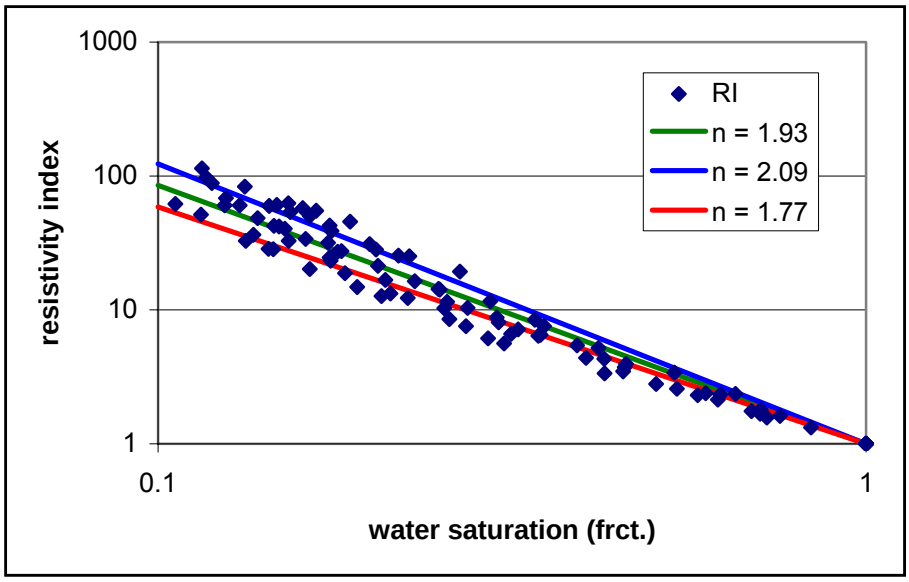

Figure B9a
The Archie Resistivity Index measurements are plotted together with the P50, P90 and P10 estimates of saturation exponent "n".

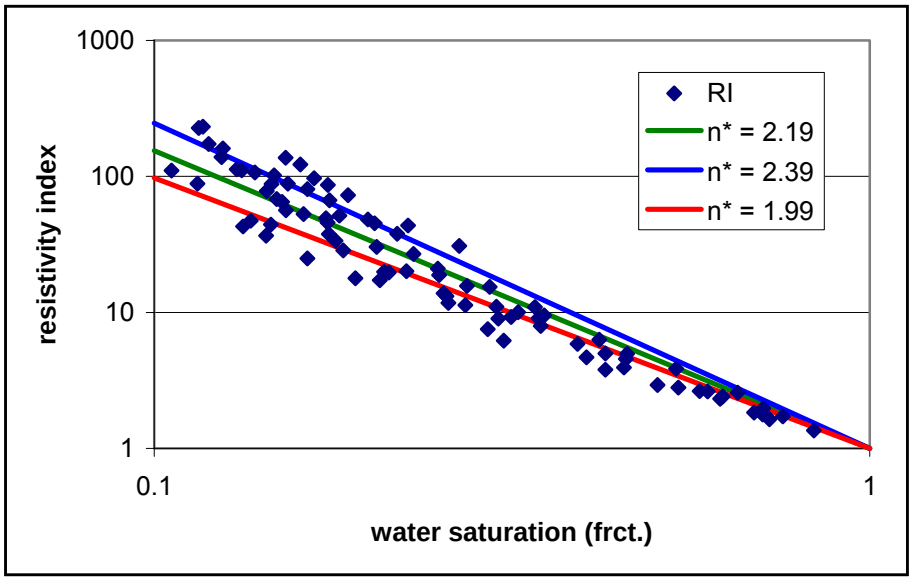

Figure B9b
The Waxman-Smits Resistivity Index measurements are plotted together with the P50, P90 and P10 estimates of saturation exponent "n".*

2.10 Irreducible Water Saturation

Capillary pressure measurements suitable for determination of irreducible water saturation have been carried out on 12 samples from Sole-2. These are 12 porous plate (pressure equilibrium) capillary pressure curves.

Figure B10a shows the relationship between the porosity and irreducible water saturation. There is a wide scatter in the data, with an apparently anomalous point at porosity near 0.20. This point has been excluded when calculating the P10, P50 and P90 relationships shown. The equation of the P50 line is:

$$S_{wirr} = 0.007 \cdot \phi^{-2.52}$$

where ϕ is expressed as a fraction of bulk volume and Swirr as a fraction of pore volume. Note that the uncertainty for P90/P10 purposes is ±41% when the apparently anomalous point at porosity near 0.20 is neglected. Inclusion of this point increases the uncertainty at the P90/P10 to ±49%.

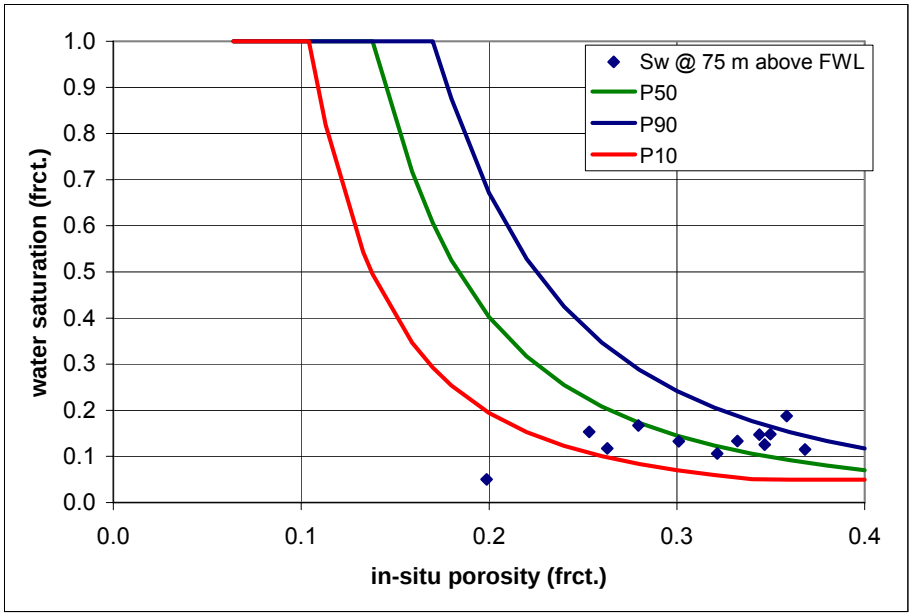

Figure B10a
The irreducible water saturations from air-brine capillary pressure measurements are plotted as a function of porosity.

Figure B10b shows the relationship between the permeability and irreducible water saturation. It is clear that there is a much better correlation than with porosity, resulting in the narrow spread in the P10, P50 and P90 relationships shown. The equation of the P50 line is:

$$S_{wirr} = 0.987 \cdot k^{-0.265}$$

where k is in milliDarcies and Swirr is expressed as a fraction of pore volume. Note that the uncertainty for P90/P10 purposes is ±26%.

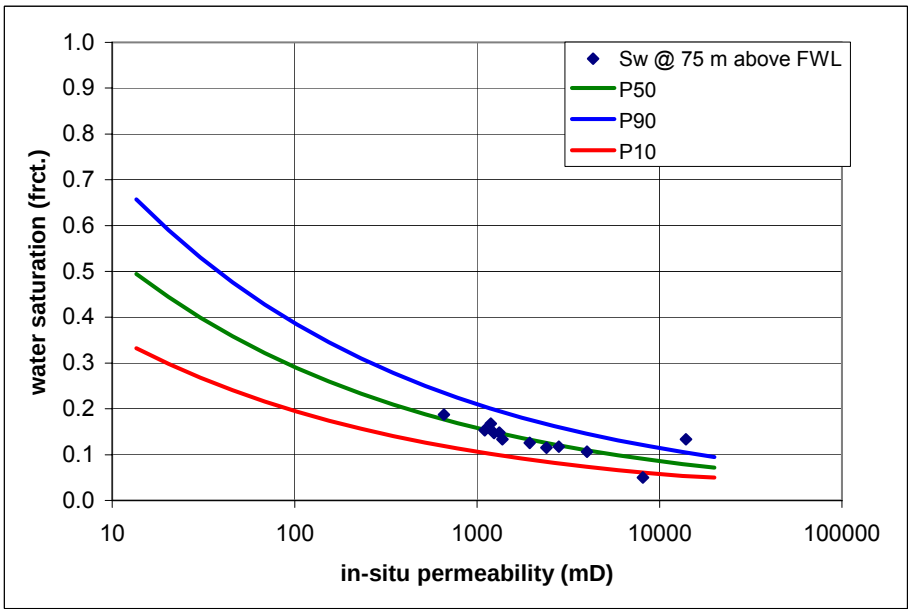

Figure B10b
The irreducible water saturations from air-brine capillary pressure measurements are plotted as a function of permeability.

2.11 Capillary Pressures

All the capillary pressure data has been compiled and converted to height above a FWL using the equations below:

$$h = (\sigma\cdot\cos\theta)_{is}/(\sigma\cdot\cos\theta)_{lab} \cdot 6895\cdot P_c/(9.81\cdot(\rho_{water}-\rho_{gas})) \quad 1$$

where h is the height above the FWL in m, $(\sigma\cdot\cos\theta)_{is}$ and $(\sigma\cdot\cos\theta)_{lab}$ are the fluid surface tensions multiplied by the appropriate fluid contact angles at stressed and laboratory conditions respectively. The capillary pressure P_c is expressed in psi, while the stressed reservoir water and gas densities are expressed in kg/m^3. The factor 9.81 is g (the Earth's gravitational constant in m/s^2) and the factor 6895 is required for the conversion of psi to Pa.

For the laboratory measurements and the reservoir conditions observed in the Sole Field, the following values have been used:

air-brine measurements in lab.:	$(\sigma\cdot\cos\theta)_{lab}$ = 72.0 (standard value)
gas-brine in reservoir:	$(\sigma\cdot\cos\theta)_{is}$ = 50.0 (standard value)
in-situ water density:	ρ_{water} = 1015.9 kg/m^3 (Ion, 2003)
in-situ gas density:	ρ_{gas} = 59.8 kg/m^3 (Ion, 2003)

The data has also been subdivided into the high (Facies 1) and low (Facies 2) gamma ray facies to see if such a subdivision will improve saturation-height function matches with core measurements.

Porosity Based Saturation-Height Modelling

Figure B11a shows the available capillary pressure data for Facies 1, while Figure B11b shows the capillary pressure data for Facies 2. Both Figures use porosity in the legend. The high GR Facies groups very closely, showing little variation, while the low GR Facies shows one capillary pressure curve with very low irreducible water saturations.

These Figures also clearly show that the variation in capillary pressure curve shape is inconsistent with porosity in either Facies. Use of porosity to determine saturation-height behaviour will be most effective using an average curve, such as that shown in Figure B11c. Two saturation-height functions are also shown attempting to model the average curve. The Thomeer model is clearly better than the Lambda formula. The formula of the Thomeer model is given below:

$$S_w = 1-a\cdot\exp[-g/(h/h_d)]$$

where a= 1.032, g = 0.424 and h_d = 0.190, h is the height above the FWL in metres and S_w is the water saturation expressed as a fraction of pore volume. Note that the uncertainty in water saturations estimated using this relationship is ±0.116 at the P90/P10 levels. Also note that this function is only valid for heights up to around 80 m above the FWL.

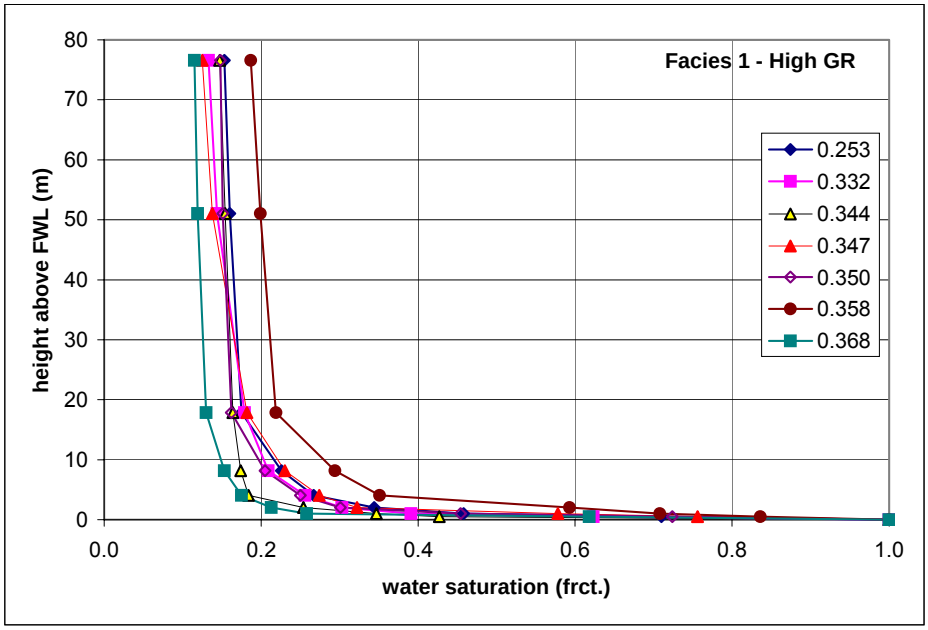

Figure B11a
The air-brine capillary pressure measurements for the high GR Facies are plotted using porosity in the legend.

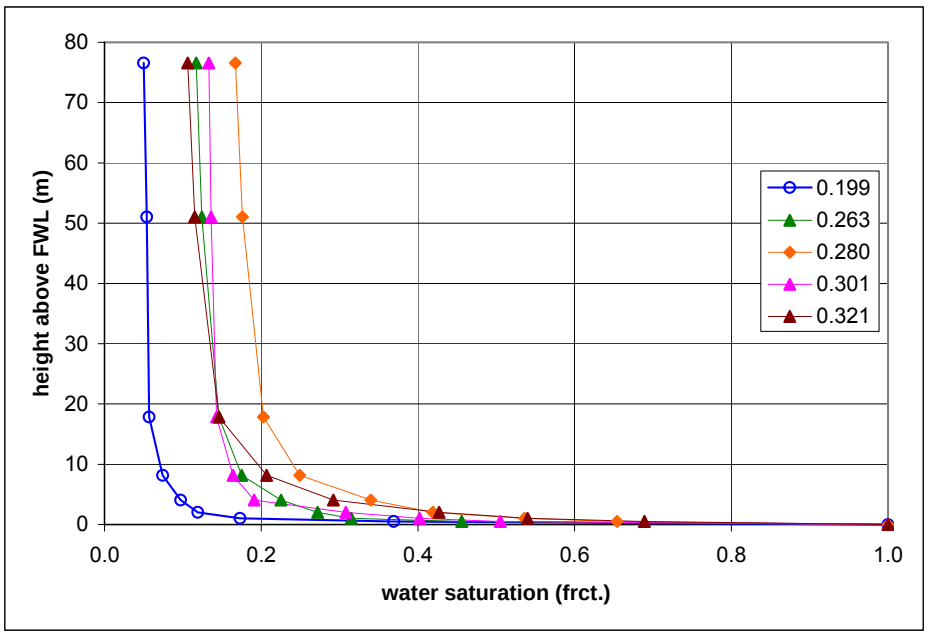

Figure B11b
The air-brine capillary pressure measurements for the low GR Facies are plotted using porosity in the legend.

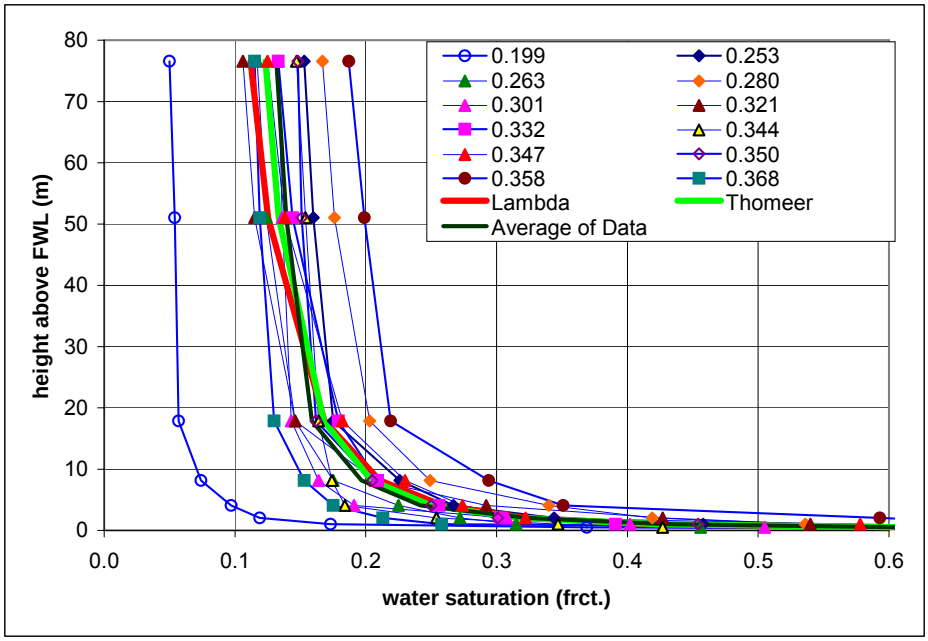

Figure B11c
The air-brine capillary pressure measurements for the both Facies are compared with an average capillary pressure curve (black line) and saturation-height functions modelling the average (red and green lines).

Permeability Based Saturation-Height Modelling

When the data are considered using permeability instead of porosity as in Figures B11d and 11e for the high and low GR Facies respectively, more useful relationships are suggested. There is a reasonably smooth variation in capillary pressure curve shape with permeability, suggesting permeability based saturation-height functions should be satisfactory.

Two different approaches have been attempted to model the saturation-height behaviour exhibited in the capillary pressure data. The first model developed different saturation-height functions for the two Facies, while the second model used a single relationship for both Facies. Note also that Lambda, Thomeer and Leverett-J based saturation-height functions have been attempted for each model. Only the results of the best models are contained in this report, although the other models are available in the supporting files (capcurvese.xls).

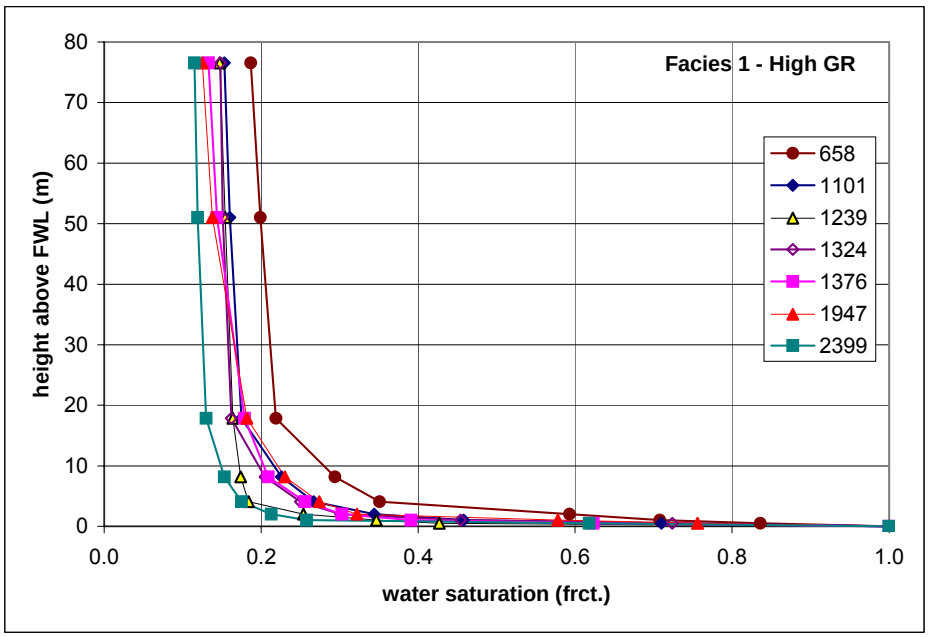

Figure B11d
The air-brine capillary pressure measurements for the high GR Facies are plotted using permeability in the legend.

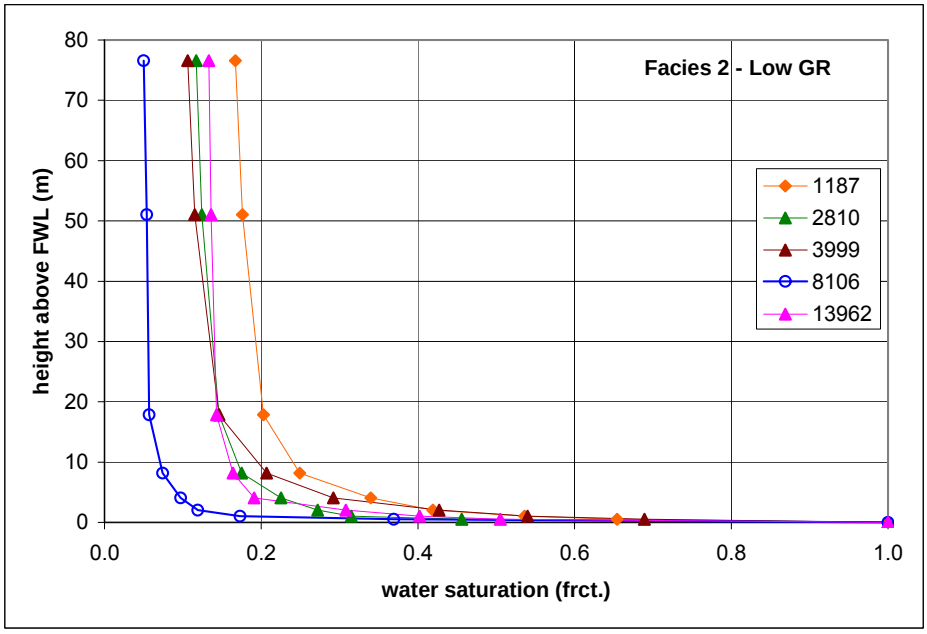

Figure B11e
The air-brine capillary pressure measurements for the low GR Facies are plotted using permeability in the legend.

Facies Based Saturation-Height Modelling

After attempting Lambda, Thomeer and Leverett-J saturation-height models, it was clear that the lowest deviations from the measured capillary pressure data were obtained with the Lambda formula for both Facies. Figures B11f and B11g compare the resulting saturation-height functions with representative sets of the measured data from each Facies. The formulae required are:

$S_w = a \cdot (h - h_d)^{-\lambda}$

where for Facies 1 (high GR): $a = -0.489 \cdot \log(K_{is}) + 1.916$

$\lambda = -0.040 \cdot \log(K_{is}) + 0.39$

$h_d = 0.420 \cdot \log(Kis) - 0.939$

and for Facies 2 (low GR): $a = -0.174 \cdot \log(K_{is}) + 0.996$

$\lambda = 0.087 \cdot \log(K_{is}) + 0.003$

$h_d = 0.039 \cdot \log(Kis) + 0.082$

where K_{is} is the permeability expressed in milliDarcies, h is the height above the FWL in metres and S_w is the water saturation expressed as a fraction of pore volume. Note that the uncertainty for P90/P10 purposes is ±0.085 for Facies 1 (high GR) and ±0.096 for Facies 2 (low GR). Also note that this function is only valid for permeabilities from 100 to 20000 mD.

For completeness, the uncertainties for the Thomeer and Leverett-J models were ±0.087 and ±0.097 respectively at the same P90/P10 levels for Facies 1 (high GR) and ±0.097 and ±0.106 for Facies 2 (low GR).

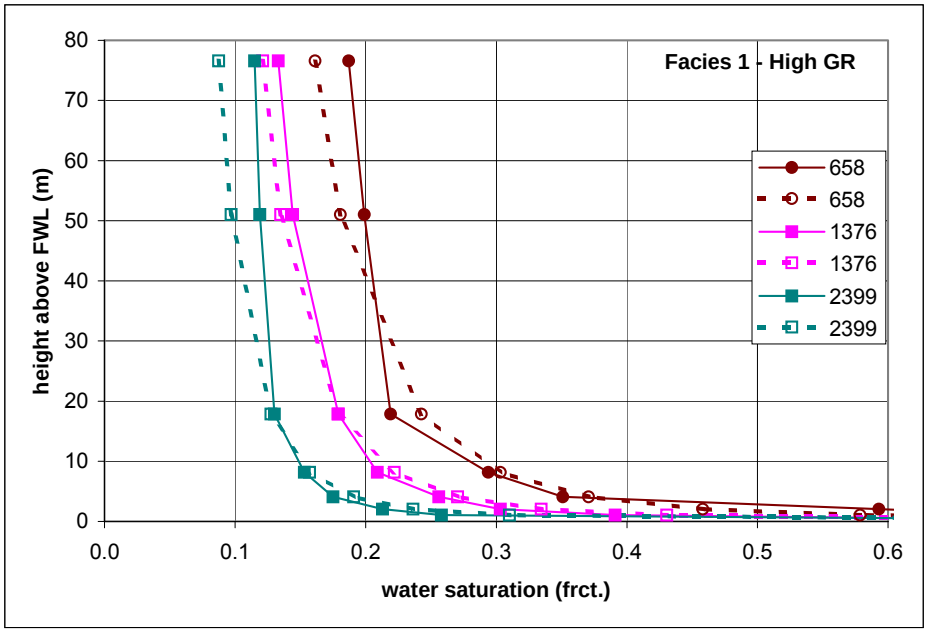

Figure B11f
A representative selection of the air-brine capillary pressure measurements for the high GR Facies are compared with their permeability based saturation-height function equivalents.

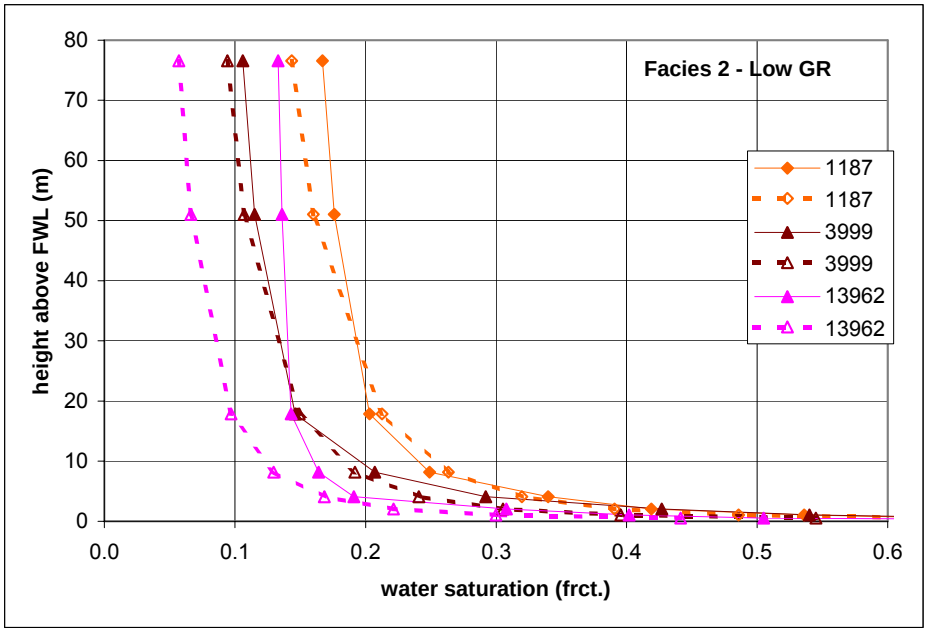

Figure B11g
A representative selection of the air-brine capillary pressure measurements for the low GR Facies are compared with their permeability based saturation-height function equivalents.

No Facies Saturation-Height Modelling

After attempting Lambda, Thomeer and Leverett-J saturation-height models, it was clear that the lowest deviations from the measured capillary pressure data were obtained with the Thomeer formula. The resulting saturation-height function is described below and compared with a representative set of the measured data in Figure B11h.

$$S_w = 1-a\cdot\exp[-g/(h/h_d)]$$

where $a = 0.059\cdot\log(K_{is}) + 0.851$

$g = -0.005\cdot \log(K_{is}) + 0.481$

$h_d = 10^{-0.350\cdot \log(Kis) +0.394}$

where K_{is} is the permeability in milliDarcies, h is the height above the FWL in metres and S_w is the water saturation expressed as a fraction of pore volume. Note that the uncertainty for P90/P10 purposes is ±0.094. Also note that this function is only valid for heights up to around 80 m above the FWL and for permeabilities from 100 to 20000 mD.

For completeness, the uncertainties for the Lambda and Leverett-J models were ±0.096 and ±0.102 respectively at the same P90/P10 levels.

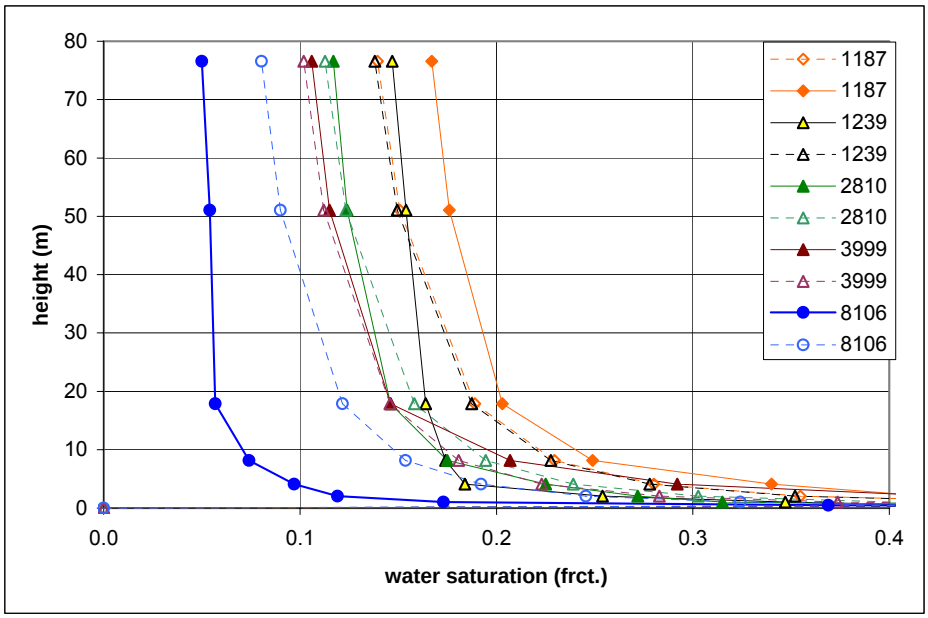

Figure B11h
A representative selection of the air-brine capillary pressure measurements are compared with their permeability based saturation-height function equivalents.

2.12 Residual Gas Saturations

Since reasonable aquifer support is expected, attempts have been made to quantify residual gas saturations based on Special Core Analyses (SCAL). Initially, experiments run were: air-brine counter-current imbibition (4 samples) and air-brine centrifuge forced imbibition capillary pressure curves at net overburden pressure (13 samples). The results are shown in Figure B12, in an initial vs. residual form as used by Land (1968).

As has been documented elsewhere (Adams et al, 2000), the end-points of the air-brine centrifuge experiments are considered as optimistic estimates of residual hydrocarbon saturations. Hence these values have been used to determine the P10 relationship.

The counter-current imbibition data is best interpreted by looking at the lowermost “envelope” of the data, since water sweep through samples in these experiments may be incomplete. The relationship derived in this way should be considered as the P90 case.

Four decane-brine centrifuge experiments were also carried out at this author’s suggestion, these being optimal for determining residual hydrocarbon saturations. This data is also shown on Figure B12, and has been selected as the P50 relationship. The Land (1968) relationships selected are consequently:

P50: $S_{gr} = 1/(5.26+1/(1-S_{wi}))$,

P90: $S_{gr} = 1/(2.98+1/(1-S_{wi}))$,

P10: $S_{gr} = 1/(11.0+1/(1-S_{wi}))$,

where S_{wi} is the initial water saturation and S_{gr} is the residual gas saturation both expressed as a fraction of pore volume.

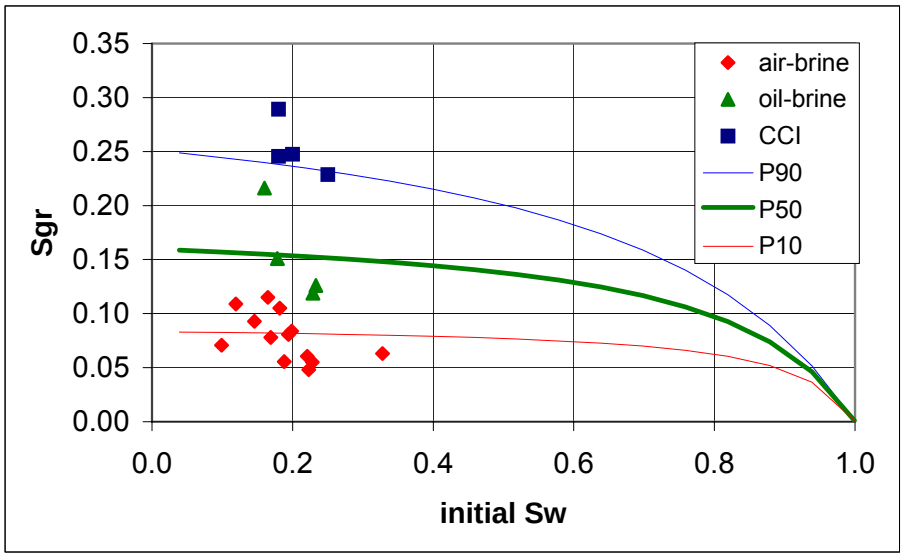

Figure B12
The various residual gas saturation experiment results are compared and the likely relationships shown.

2.13 Relative Permeability

End-point centrifuge relative permeabilities have been acquired on 13 samples from Sole-2. The experiments have been interpreted to yield the in-situ fluid permeabilities for gas and water in their mobile phases. Figures B13a and B13b show the relationships derived.

The relationship derived between the in-situ gas permeability and the in-situ gas permeability at irreducible water saturation (Figure B13a) is:

$$K_{gas} = 0.362 \cdot Kis^{1.112}$$

where K_{is} is the in-situ gas permeability in milliDarcies and K_{gas} is the in-situ gas permeability at irreducible water saturation. The uncertainty in the estimate of K_{gas} is ±14% at the P90/P10 levels.

The relationship derived between the in-situ gas permeability and the in-situ water permeability at residual gas saturation (Figure B13b) is:

$$K_w = 0.686 \cdot Kis^{0.965}$$

where K_{is} is the in-situ gas permeability in milliDarcies and K_w is the in-situ water permeability at residual gas saturation i.e. in the “swept” zones. The uncertainty in the estimate of K_w is ±19% at the P90/P10 levels.

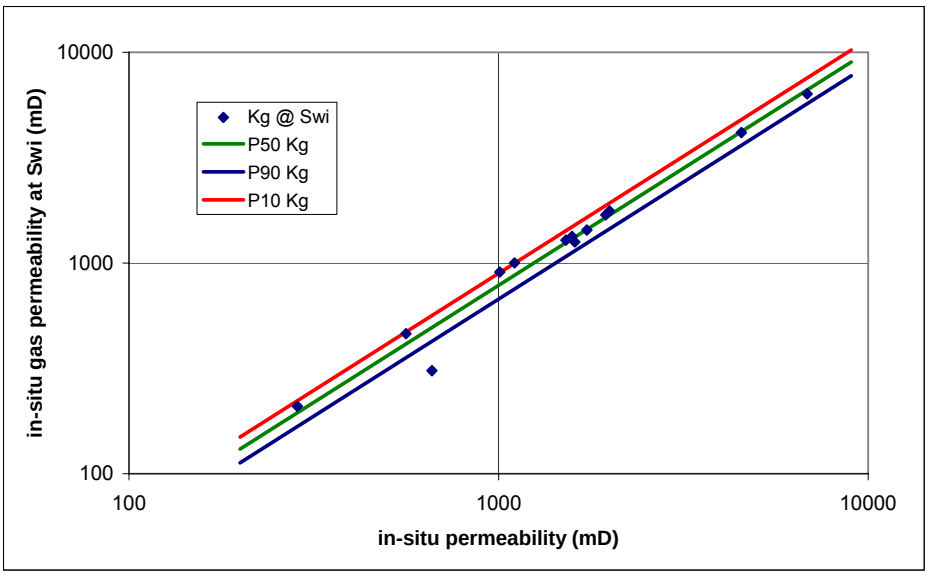

Figure B13a
The relationship between in-situ permeability and in-situ gas permeability at irreducible water saturation i.e. gas permeability when the rock contains as much gas as possible.

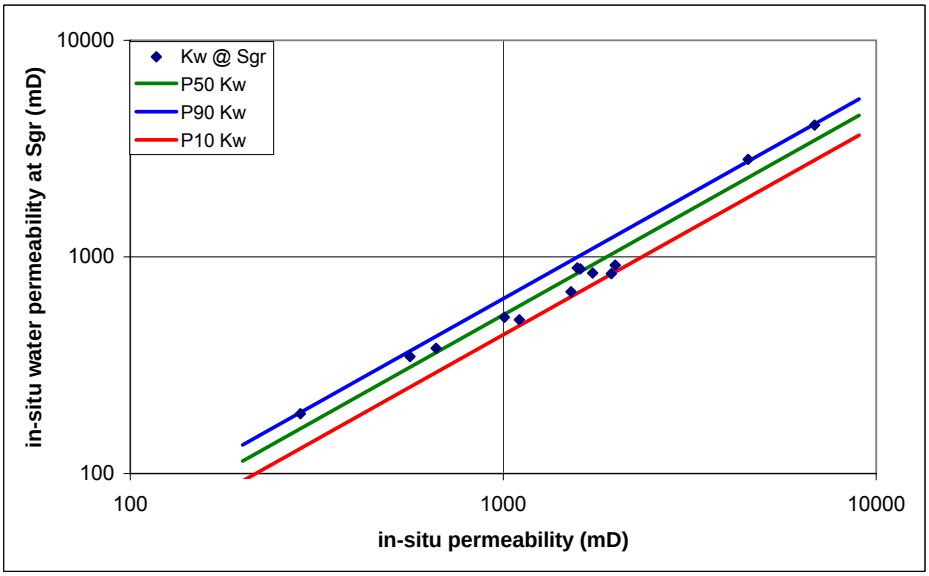

Figure B13b
The relationship between in-situ permeability and in-situ water permeability at residual gas saturation i.e. water permeability through "swept" zones.

3 PETROPHYSICAL EVALUATION

The following section describes the methodology recommended for petrophysical evaluation of wells in the Sole Field area. It has been tested on the cored well Sole-2 before being applied to the other wells Sole-1, Dart-1, Hammerhead-1 and Leatherjacket-1.

3.1 Normalisation

Since Sole-2 was cored, this well has been used as the baseline against which other wells have been calibrated. Changes have been made such that the non-reservoir sealing unit above the gas-bearing Latrobe Formation has similar log responses in all wells. It is reasoned that the seal unit is unlikely to exhibit significant property variations over the Sole Field area.

Below details the logs normalised, the changes made and their justifications. The normalisations are shown in Figures B14a, B14b, B14c and B14d.

Table B2 ***The logs normalised during the course of this study. Sole-2 was used as the baseline (12 ¼" hole).***

Well	Log	Change	Justification
Sole-1 (1973, 9 $^{7}/_{8}$" hole)	GR	0.66·GR+26.2	To match GR above Latrobe and peaks within Latrobe in Sole-2
Hammerhead-1 (1982, 8 ½" hole)	GR	1.19·GR+12.4	To match GR above Latrobe and peaks within Latrobe in Sole-2
Leatherjacket-1 (1986, 12 ¼" hole)	GR	1.12·GR+15.3	To match GR above Latrobe and peaks within Latrobe in Sole-2
Dart-1 (1973, 9 $^{7}/_{8}$" hole)	GR	1.06·GR+9.7	To match GR above Latrobe and peaks within Latrobe in Sole-2

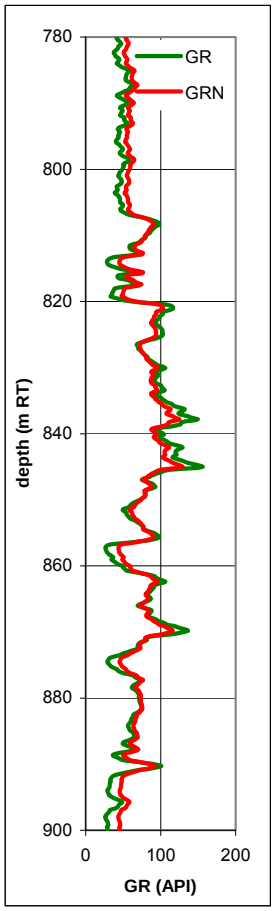

Figure B14a *– GR before and after normalisation for Sole-1.*

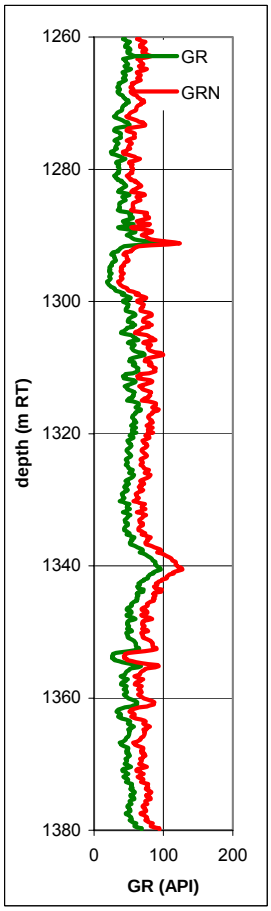

Figure B14b *– GR before and after normalisation for Hammerhead-1.*

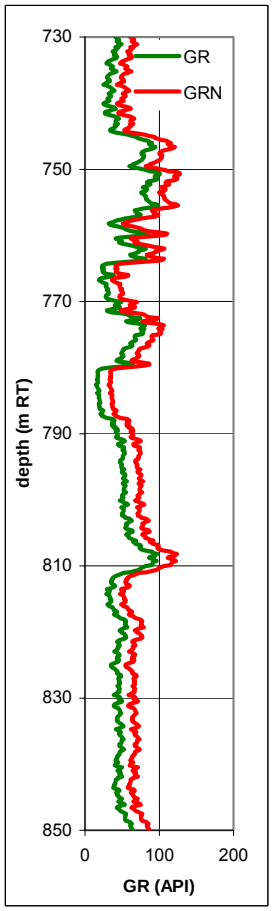

Figure B14c *– GR before and after normalisation for Leatherjacket-1.*

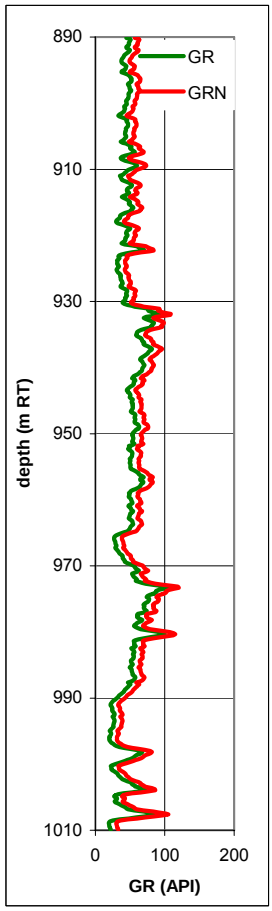

Figure B14d *– GR before and after normalisation for Dart-1.*

3.2 Temperature

For log interpretation purposes the temperatures actually recorded in the wells during the resistivity logging runs were used, this being the environment in which the logs were actually operating.

3.3 Porosity

Ideally, porosity should be calculated using the density log, correcting for the presence of hydrocarbons using an iterative procedure involving the invaded zone resistivity. For the Sole Field, the required parameters for this calculation are the grain density (2.647 g/cc from §2.1) and the gas density (0.0598 g/cc see §2.9).

When the density log quality is poor, the next best tool for estimating porosity is the sonic log. Use of standard sandstone sonic values (Δt_{ma} = 54 μs/ft and Δt_{fl} = 182 μs/ft) produces porosities that are too high (see *Figure B15a*), suggesting that local calibration to the density porosity is required – as is usually the case.

This calibration has been carried out using the logs from Dart-1 and from below the FWL in Sole-2 – the shallower Sole-2 logs were poor owing to cycle skipping on the sonic and hole rugosity on the density. Figure B15a shows the correlation derived, while the equation is below:

$$\phi_{son} = 0.0052 \cdot DT - 0.30,$$

where DT is the sonic transit time expressed in microseconds per foot and ϕ_{son} is the sonic porosity expressed as a fraction of pore volume. The uncertainty in porosity estimates is ±0.036 at the P90/P10 levels.

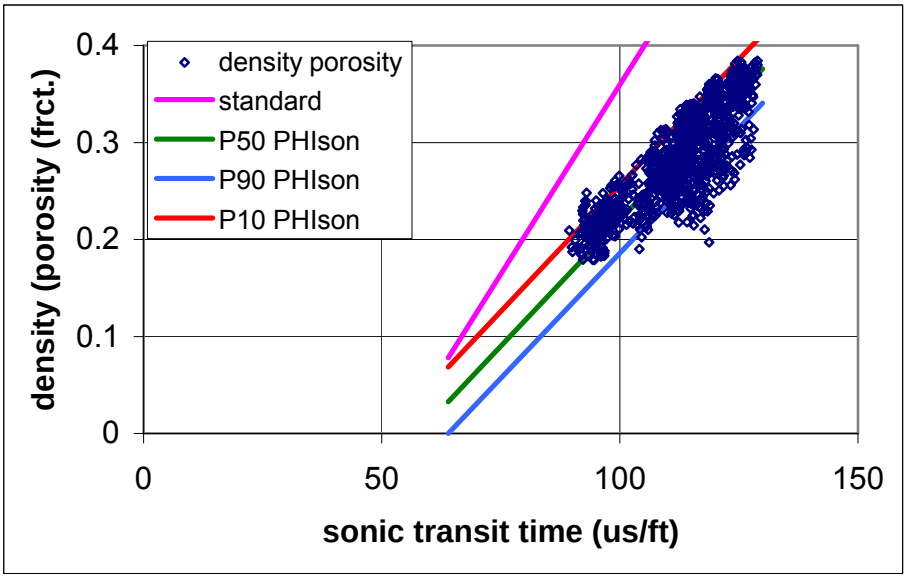

Figure B15a
The derivation of porosity from the Sole-2 and Dart-1 sonic logs. Note that use of standard sonic porosity parameters is inappropriate.

In Sole-2, the sonic log is clearly cycle skipping through the gas zone rendering the log unusable over this interval. The density log also has intervals showing rugosity in the gas. Hence a porosity relationship using the normalised GR log has been derived. Calibration of the normalised gamma ray to the core porosities has been carried out to create the model. Figure B15b illustrates the correlation produced. The relationships derived are given below:

$$\phi_{highGR} = 0.388\text{-}0.00037 \cdot GR ,$$

$$\phi_{lowGR} = 0.347\text{-}0.00067 \cdot GR ,$$

$$S_{GR} = 1/(1+10^{((86-GR)\cdot(-0.1))}) ,$$

$$\phi_{GR} = \phi_{lowGR} \cdot (S_{GR}) + \phi_{highGR} \cdot (1-S_{GR}) ,$$

where GR is the normalised GR log reading, ϕ_{lowGR} is the GR porosity for the low gamma ray sands, ϕ_{highGR} is the GR porosity for the high GR sands and ϕ_{GR} is the combined GR based porosity. Note that a Sigmoidal scaling factor (S_{GR}) has been constructed so as to provide a smooth transition when moving from high or low GR sands to the other sand type. The uncertainty in porosities derived using this model is ±0.04 at the P90/P10 levels, only slightly more than for the sonic porosity.

Note that detailed uncertainty analysis of the density porosity is discussed in §5.1 and §5.9.

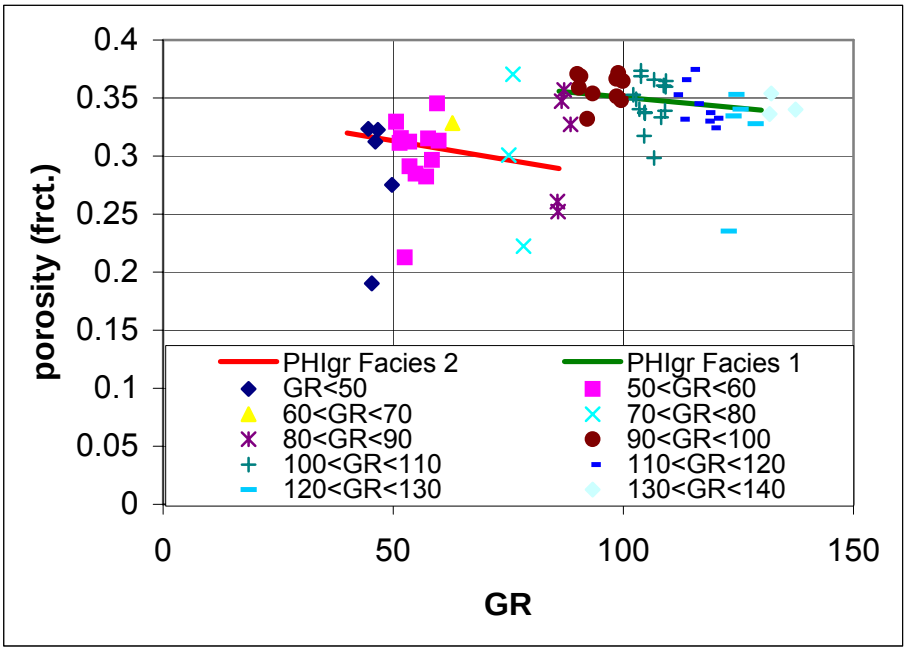

Figure B15b
The derivation of porosity from the Sole-2 (baseline) gamma ray log, based on core porosities.

3.4 Permeability

The procedure outlined in §2.4 should be used to estimate permeability, i.e.:

i) Estimate the shale fraction from the GR log $V_{sh} = (GR-GR_0)/(GR_1- GR_0)$, where GR is the gamma ray log response, GR_0 =-4 and GR1 =177.

ii) Calculate an effective porosity $\phi_e = \phi_t \cdot (1-V_{sh})$, where ϕ_t is the total porosity estimated from the density log.

iii) Lastly, calculate the in-situ fluid (gas) permeability $K_{is} = 10^{(7.29 \cdot \phi e + 2.24)}$

3.5 True Formation Resistivity

Where data is available, true formation resistivity has been estimated by first applying the standard Schlumberger borehole corrections followed by the appropriate invasion correction algorithms. For the latest Platform Express logs from Schlumberger, these corrections were carried out by the logging contractor.

3.6 Formation Water Resistivity

Detailed discussion of the formation water salinity is made in §5.6. In this section, the primary objective of this study, being the Sole gas accumulation is discussed.

The water leg in Sole-2, provides sufficient good quality log data to allow the Formation Water salinity to be estimated using the apparent formation water resistivity approach, Figure B16 shows a histogram of the formation water salinity estimates in the water leg. The mode is 33000 ppm NaCl eq. and this value is recommended as

the formation water salinity to use for petrophysical evaluation in the absence of a formation water sample. Note that there is no bimodality apparent in the histogram suggesting either fresher or more saline formation water to have a significant influence.

The uncertainty at the P90/P10 levels is ± 7000 ppm NaCl equivalent.

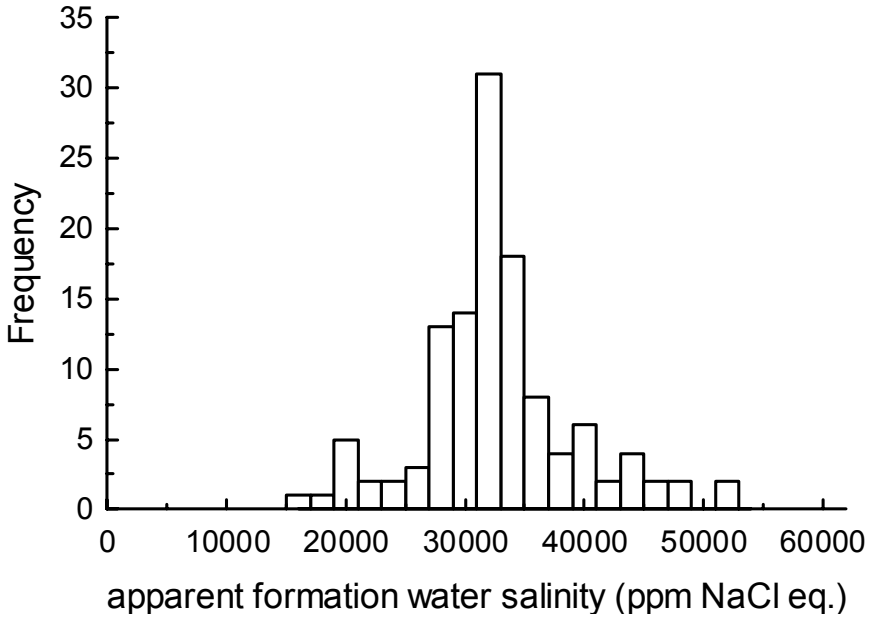

Figure B16
Histogram of the apparent formation water salinity from the water-leg in Sole-2.

3.7 Hydrocarbon Saturation from Logs

Hydrocarbon saturations have been estimated using both the Archie and Waxman-Smits equations. The clay conductivity correction term derived in this report (§2.7) has been used. The cementation and saturation exponents required for these equations are those derived from the core analyses in §2.

The log evaluated reservoir intervals, porosities and water saturations were then visually examined to ascertain whether the results were consistent.

3.8 Net Sands

To determine net sand criterion, calculations were initially made with no non-reservoir lithologies defined. Consistent criteria were then sought for all wells in the study allowing sand to be differentiated from non-reservoir.

Owing to the radioactive nature of some of the sands, the GR log could not be used on its own for non-reservoir identification.

The preferred tool for non-reservoir differentiation is the normalised density-neutron log separation. Typically, where $(\phi_n-\phi_d)/\phi_d$ is greater than 0.8, the lithology is non-reservoir. This hypothesis has been tested in Sole-1 and Sole-2 as shown in *Figures B17a* and *B17b* by examining the impact of varying the lithology cut-off. Changes are clearly significant up to a value of 1.0. Above this point, there is negligible value additional net sand gained by increasing the lithology cut-off. Hence, this value for the lithology cut-off has been selected for the Sole Field. The gamma ray, resistivity log separation, the SP log and the mud log have been used to confirm that all the reservoir has been defined using this lithology cut-off.

Sums and averages reported are based on this net sand definition. All reservoir (net sand) above the FWL is considered as pay.

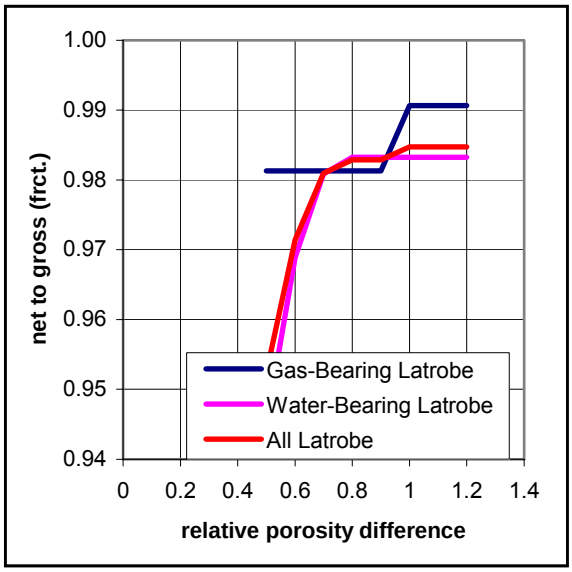

Figure B17a – *The effect of lithology cut-off of net-to-gross in Sole-1. A value around 1.0 is recommended.*

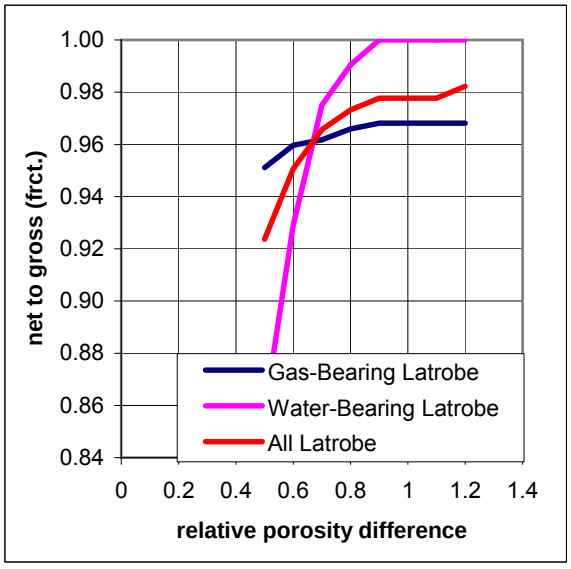

Figure B17b – *The effect of lithology cut-off of net-to-gross in Sole-2. A value between 0.9 and 1.0 is recommended.*

4 INDIVIDUAL WELLS

Full log data is available for Sole-2, Sole-1, Dart-1, Hammerhead-1 and Leatherjacket-1.

These wells have been quantitatively evaluated over the Latrobe Formation, allowing this reservoir unit to be characterised in the Sole Field vicinity. The results from each well evaluation are reported in the following sections, while Appendix B3 contains the summary statistics for each well and Appendices 3a to 3e contain the log displays. Note that Appendix B2 explains the log name conventions used.

4.1 Sole-2

Sole-2 was drilled by OMV in 2002 as an appraisal well on the Sole-1 gas discovery. It found the Latrobe Formation gas-bearing from 770.0 to 841.6 m RT (745.0 to 816.6 mss). Average porosities are 30.3 % with gas saturations of 85%. Net sand is 69.3 m (net-to-gross of 97%).

The uncertainty on the log quality has resulted in a range of gas thicknesses for Sole-2 from 70.5metres 73metres. A most likely thickness of 71.6metres has been used for the petrophysics. The use of 70.5 metres for the gas thickness at Sole-2 in the field mapping results in a conservative approach.

Formation pressure data confirms the presence of gas with a clear gas gradient through the Latrobe Formation down to 841.6 m RT (816.6 mss). Note that the capillary pressure data confirms this depth as the likely FWL. The USI log run after casing and cementing also noted gas-cut cement down to 841.6 m RT (816.6 mss), with no gas indications deeper.

There are two major issues that have been addressed in the Sole-2 log evaluation. The first issue is concerned with the match between log and core derived porosities and is discussed in §5.1. The second matter relates to the resistivity response at the base of the hydrocarbon column in Sole-2 and is discussed in §5.4. The base case numbers are those reported here.

4.2 Sole-1

In 1973, Sole-1 discovered the Latrobe Formation gas-bearing from 810 to 827.9 m RT (800.2 to 818.1 mss). The location of the GWC is confirmed on the logs by the gas effect on the neutron and the cycle skipping on the sonic log both disappearing around 827.9 m RT (818.1 mss).

The range in gas thickness seen from the logs in Sole-1 is 17.8metres to 18.0 metres. A most likely thickness of 17.9metres has been used for the petrophysics. The use of 18.0 instead of 17.8 meters for the gas thickness at Sole-1 in the field mapping has a minimal impact on GRV.

Average porosities are 32.6% with gas saturations of 66%. Net sand is 18.0 m (net-to-gross of 100%).

Note that the resistivity log cannot be corrected for invasion owing to the absence of meaningful shallower reading logs. There are also a number of artefacts in the induction log response that have been previously identified as “polarisation horns” (Koelimij, 2001). Unfortunately, the induction tool is a conductivity “seeking” device and will read artificially low resistivities through these intervals. Hence, through the gas column, the maximum values of either the deep induction or the short normal resistivities have been used in an attempt to improve the resistivity log response.

4.3 Hammerhead-1

Drilled by Shell in 1982, Hammerhead-1 encountered a thick Latrobe sequence, but found no hydrocarbon-bearing units. The well was plugged and abandoned on completion of wireline logging.

The upper part of the Latrobe Formation, equivalent to the gas-bearing interval in the Sole Field, from 1291-1383 m RT (1269-1361 mss) has average porosities of 27.7 % while net sand is 92.2 m (net-to-gross of 100%).

Implications regarding formation water salinity from Hammerhead-1 are discussed in §5.6.

4.4 Leatherjacket-1

Drilled in 1986 by Esso, Leatherjacket-1 targeted the Latrobe Group in a dominantly fault dependant closure situated on the high side of a NE-SW trending inverted normal fault. Hydrocarbons were encountered in three zones and interpreted as oil after formation pressures and oil samples were recovered.

The presence of residual hydrocarbons is evidenced by the invaded zone saturations. Use of a formation water salinity at 15,000 ppm NaCl eq. (from the adjacent silts and shales) produces oil saturations for the reservoir close to those seen in the invaded zone for the residual column, confirming its presence.

The uppermost interval of interest is from 763.8-772.7 m RT (742.8-751.7 mss) and has average porosities of 30.3% and oil saturations of 60% while net sand is 8.3 m (net-to-gross of 93%). The middle oil-bearing section is from 778.5-789 m RT (757.5-768.0 mss) and has average porosities of 30.2% and oil saturations of 53% while net sand is 10.5 m (net-to-gross of 100%). The lower oil-bearing section is from 811.1-819.1 m RT (790.1-798.1 mss) and has average porosities of 26.8% and oil saturations of 53% while net sand is 8.0 m (net-to-gross of 100%).

The presence of three short columns is best explained by considering the presence of small seals and residual hydrocarbons i.e. the structure was once filled to a greater depth and was breached or otherwise spilt oil at some time in the past. The short oil columns observed are all that remains.

Note that owing to poor hole conditions, the intervening seals between these oil columns are not clear on the density-neutron separation, hence the SP log has been used to determine the seal locations over the poor hole sections.

4.5 Dart-1

Drilled in November 1973, Dart-1 was targeted at the Latrobe sandstones in a down-dip position from the Sole-1 discovery well on a postulated stratigraphic trap. The trap was not present, so although the Latrobe was found with excellent reservoir quality, no hydrocarbons were encountered.

The upper part of the Latrobe Formation from 921-991 m RT (911.2-981.2 mss) has average porosities of 31.9 % while net sand is 69.2 m (net-to-gross of 99%).

5 DISCUSSION

5.1 Porosity

Comparison between the core and density log derived porosities in Sole-2 is made in Figure B18a and B18b. It is clear that the porosities are underestimated by an average amount of 0.03 porosity units. This difference is quite large and (from Figure B18c), it is apparent that the largest differences are in the sections where the hole size becomes enlarged below 795 m RT.

Possible causes of this porosity discrepancy have been investigated and include:

i. Uncertainties associated with the positioning of the core relative to the wireline logs owing to difficulties during the coring and the poor recovery (OMV, 2002),

ii. Whole mud invasion into the permeable sands in the enlarged hole section.

iii. Invaded zone resistivity unrepresentative of volume investigated by the density log.

Since it is clear that there has been a lot of mud filtrate invasion at least, from the invasion profile through the enlarged hole and from likely gravity slumping of mud filtrate (§5.4), the most likely explanation appears to be the whole mud invasion. Such invasion would increase the density log measurements over the intervals invaded, reducing the porosities estimated significantly. Figure B18d shows supporting data for deep invasion, with evidence of mud solid invasion into the core apparent on the core photographs.

It is not possible to correct for such mud solid invasion quantitatively other than by introducing a “calibration” factor to the density porosities, scaling them to match the core data. A simple linear calibration of the existing density porosity to the core data has been carried out to correct the calculated porosities in Sole-2. Least squares analysis of the data in Figure B18a gives the formula below:

$$\phi_{Dcal} = 0.5095 \cdot \phi_D + 0.1754$$

where ϕ_D is the hydrocarbon corrected density porosity and ϕ_{Dcal} is the density porosity recalibrated to match the core porosities. Both porosities are expressed as a fraction of bulk volume. The P90/P10 uncertainties are slightly skewed being -0.04 for P90 and +0.03 for P10 and are also shown on *Figure B18a*. *Figure B18e* shows a histogram of the differences between the new log porosities and the core porosities. Note that the distribution is not quite normal, as suggested by the uncertainties. However the mean difference is zero as expected.

Using this recalibrated porosity, the average porosities in Sole-2 above the FWL increase from 26.9% to 30.3%. The average gas saturations in Sole-2 also increase from 81% to 85% with no alteration in the net-to-gross.

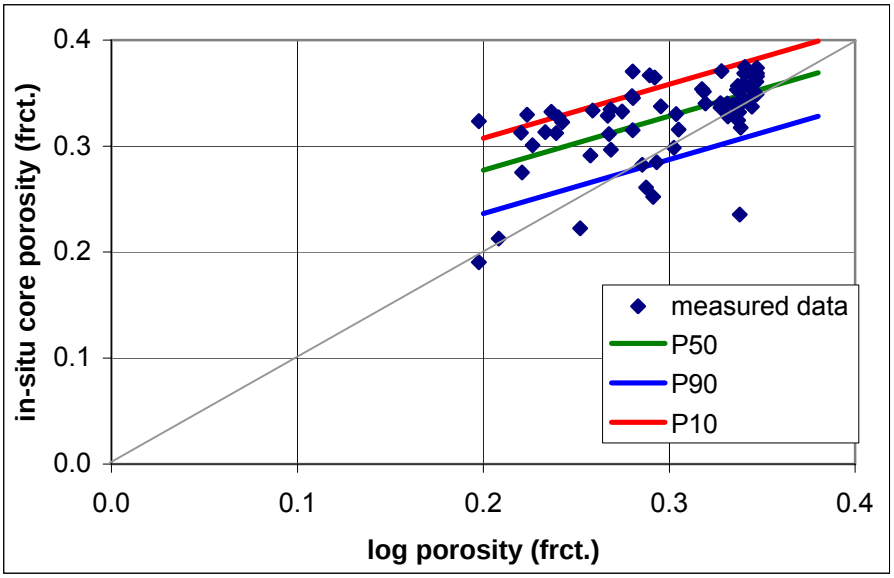

Figure B18a
Porosity from wireline logs is compared with that from core analyses for the cored section of Sole-2.

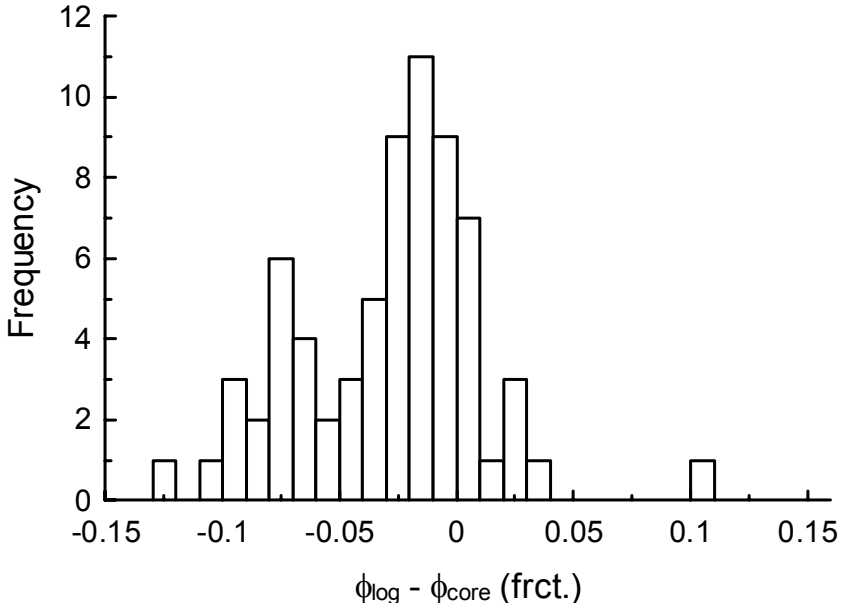

Figure B18b
The difference between the uncorrected log derived and in-situ core porosities for the Latrobe Formation in Sole-2.

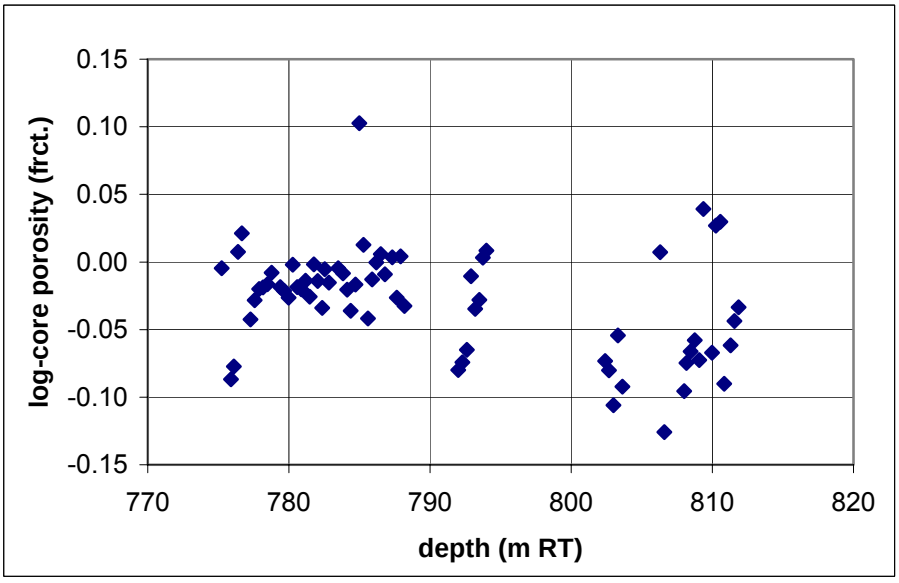

Figure B18c
The difference between the uncorrected log derived and in-situ core porosities is plotted against depth for the Latrobe Formation in Sole-2.

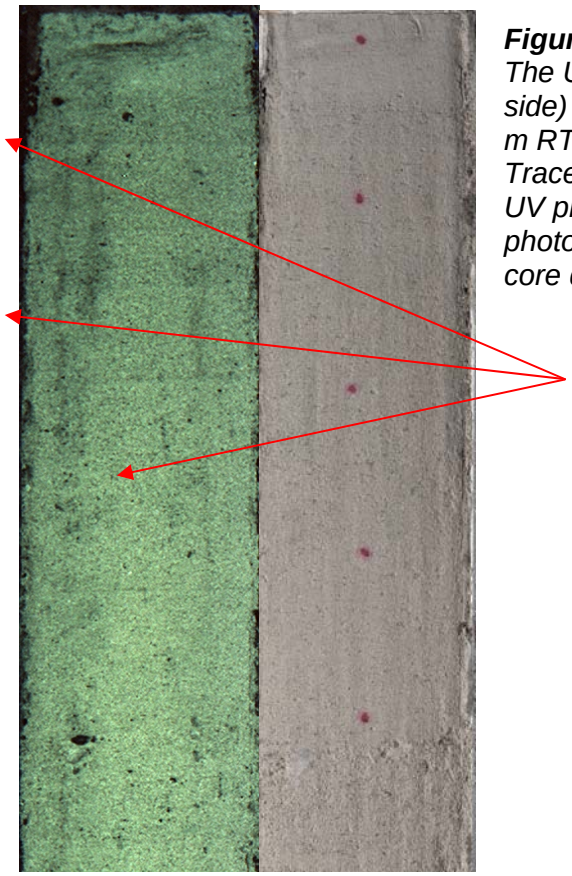

Figure B18d
The UV (on left hand side) and white light (right hand side) photographs of the core interval 805.85-806.35 m RT in Sole-2.
Traces of whole mud invasion are apparent on the UV photograph as darker lines. The white light photos illustrate that the darker zones are not due to core damage or other geological features.

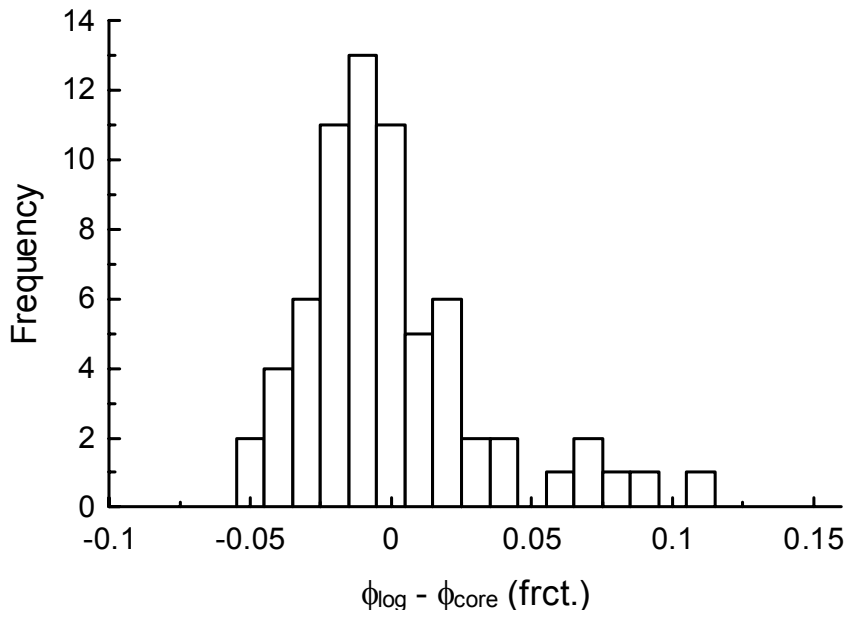

Figure B18e
The difference between the corrected log derived and in-situ core porosities for the Latrobe Formation in Sole-2.

5.2 Permeability

Comparison between the core and log derived permeabilities in Sole-2 is made in *Figure B19a* and *B19b*. The correlation appears reasonable with the mean difference being only a factor of 16%. Uncertainty analysis using the differences between the log-derived estimates and the measured data gives the P90/P10 uncertainties as a factor of 2 (i.e. $10^{0.3}$). This range, which is considered reasonably small, indicates high confidence in the permeability

Figure B19c illustrates that the permeability differences have a larger range at depths below 795 m RT in the enlarged hole sections. These differences reflect the increased uncertainty in the porosities in this interval as discussed in the preceding section.

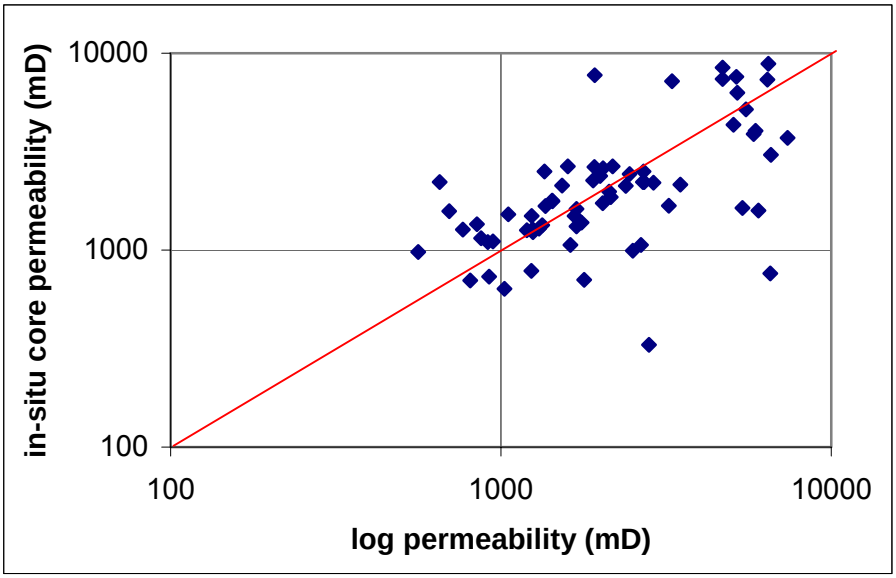

Figure B19a
Permeability from wireline logs is compared with that from core analyses for the cored section of Sole-2.

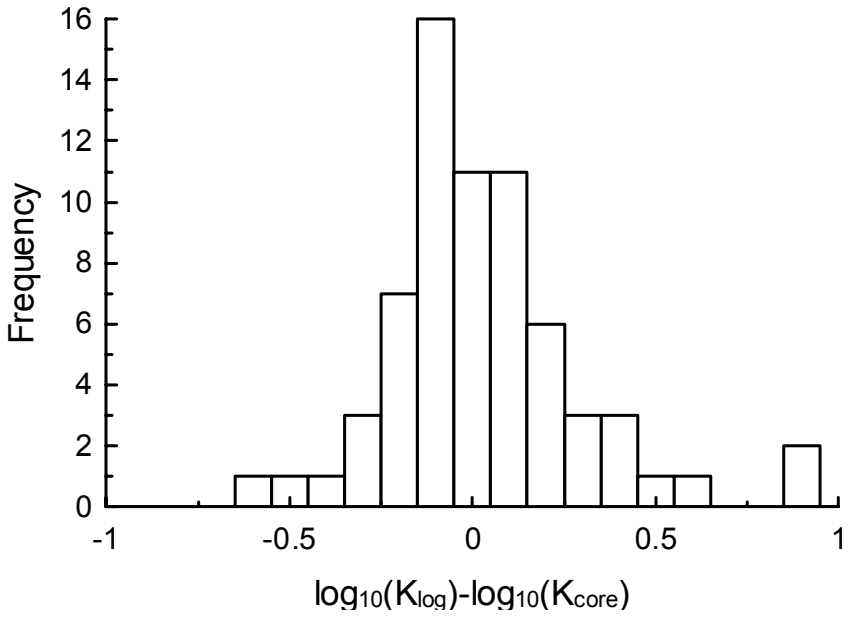

Figure B19b
The difference between the log derived and in-situ core permeabilities for the Latrobe Formation in Sole-2.

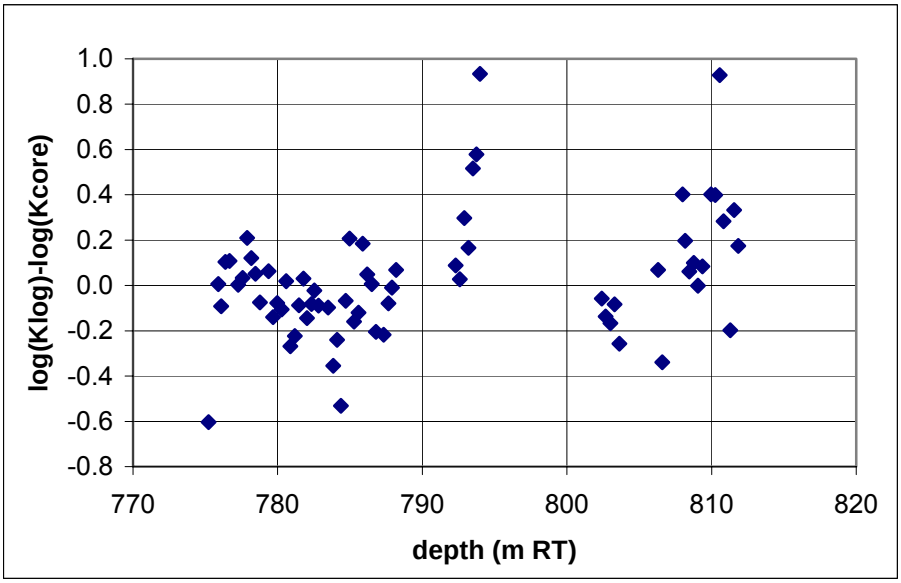

Figure B19c
The difference between the log derived and in-situ core permeabilities is plotted against depth for the Latrobe Formation in Sole-2.

5.3 Differences with Previous Evaluations

Previous petrophysical results are available for Sole-1 (Koelimij, 2002) and Sole-2 (OMV, 2002). The differences are summarised in Table B4.

In Sole-1, the average porosities are higher in this work than reported previously owing to the current porosities being total porosities as opposed to effective porosities reported previously. The hydrocarbon correction has also been more rigorous in the current evaluation. Reported hydrocarbon saturations are also slightly increased owing to use of core calibrated saturation exponents, giving an overall 11% increase in hydrocarbon column for Sole-1.

In Sole-2, the average porosities are higher in this work than reported previously owing to the calibration of the log derived porosities to the core through the washed out hole section from 795-847 m RT. The lithology definition has also been more rigorous, resulting in a 9% increase in the net sand count. Use of core based saturation exponents has resulted in a decrease in gas saturations. However, overall there is a 15% increase in hydrocarbon column.

Table B3 ***Comparisons between earlier petrophysical evaluations and the work reported herein for Sole-1 and Sole-2.***

Well	From (mRT)	To (mRT)	From (mss)	To (mss)	Gross	Net	N/G	ϕ	Sh	HCPV	Comment
Sole-1	810.0	827.9	800.2	818.1	17.9	17.9	1.00	0.303	0.643	3.507	Koelimij, 2001.
Sole-1	810.0	827.9	*800.2*	*818.1*	17.9	17.9 0%	1.00	0.326	0.663	3.885 11%	Mobile gas, this work.
Sole-2	770.0	842.8	745.0	817.8	72.8	63.3	0.87	0.279	0.880	15.550	Wellsite evaluation.
Sole-2	770.0	841.6	745.0	816.6	71.6	69.3 9%	0.97	0.303	0.850	17.836 15%	This evaluation.

5.4 Water Saturations

5.4.1 Resistivity in Sole-2 Washouts

The interval from 799 to 848 m RT in Sole-2 is washed out above 16 inches from a base of 12 ¼ inch hole. The interval from 837.2-847.2 is enlarged even further, past the 24 inch limit of the callipers. Unfortunately, this latter interval also corresponds to the location of the pressure derived FWL and adjacent gas-water contact.

Use of the measured resistivities through this interval results in gas being interpreted below the pressure derived FWL at 841.6 m RT. In an attempt to understand whether these resistivities were real or tool artefacts a simple resistivity model was constructed, using the considerations below:

i) The laterolog is a “resistivity seeking” device.

ii) The washed out borehole from 837.2-847.2 m RT contains conductive mud (Rmf ≈0.15 ohmm).

iii) The laterolog response from 837.2-847.2 m RT will be dominated by the resistivities of the adjacent (non-washed out) beds.

iv) The laterolog response from 837.2-847.2 m RT can be approximated using a distance weighted parallel resistivity summation.

A model resistivity log was constructed for the interval from 837.2-847.2 m RT using the above guidelines. This modelled profile is compared with the log response in Figure B20. The match between the two resistivities is reasonable, especially considering the model assumes that the resistivity in the washed out zone is not measured at all! Since the measured log actually does have some contribution from the formation resistivity over the enlarged hole, the model underestimates the resistivity above the GWC and overestimates below the GWC. On this basis, the resistivity log suggests a GWC near 841.6 m RT (816.6 mss), similar to that derived from the pressure data!

This simple modelling exercise implies that the deep (and shallow) resistivity log readings are significantly impacted through the washed out interval from 837.2-847.2 m RT. Hence, the log evaluation has proceeded on the assumption that FWL determined by the pressure data corresponds to the actual GWC identified using the simple resistivity model.

More detailed 3D electromagnetic modelling could verify the findings of the simple model presented here. It could also potentially invert the true formation resistivities through the enlarged hole section. An approach to Schlumberger requesting such an exercise is the recommended route to obtain such modelling results.

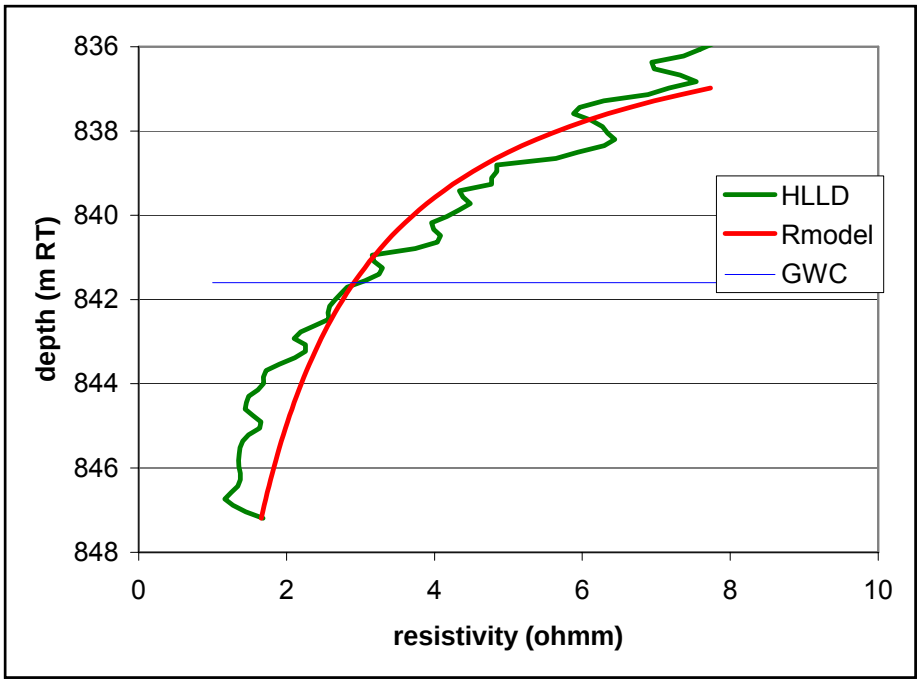

Figure B20
The modelled resistivity is compared with the measured laterolog deep response through the washed out zone from 837.2-847.2 m RT.

5.4.2 Saturation-Height Model Comparison

The differences between the log and saturation-height derived gas saturations for Sole-1 are apparent in Figure B21a and for Sole-2 in Figure B21b.

In Sole-1, the gas effect on the density-neutron log and the cycle skipping on the sonic log clearly indicate the GWC at 827.9 m RT (818.1 mss using known deviation data). Hence the saturation-height functions have been based on a FWL at this level. The match between the log-derived water saturations and those from the saturation-height functions derived in §2 is reasonable considering the vintage of the log data and the known problems with the induction log (Koelimij, 2002).

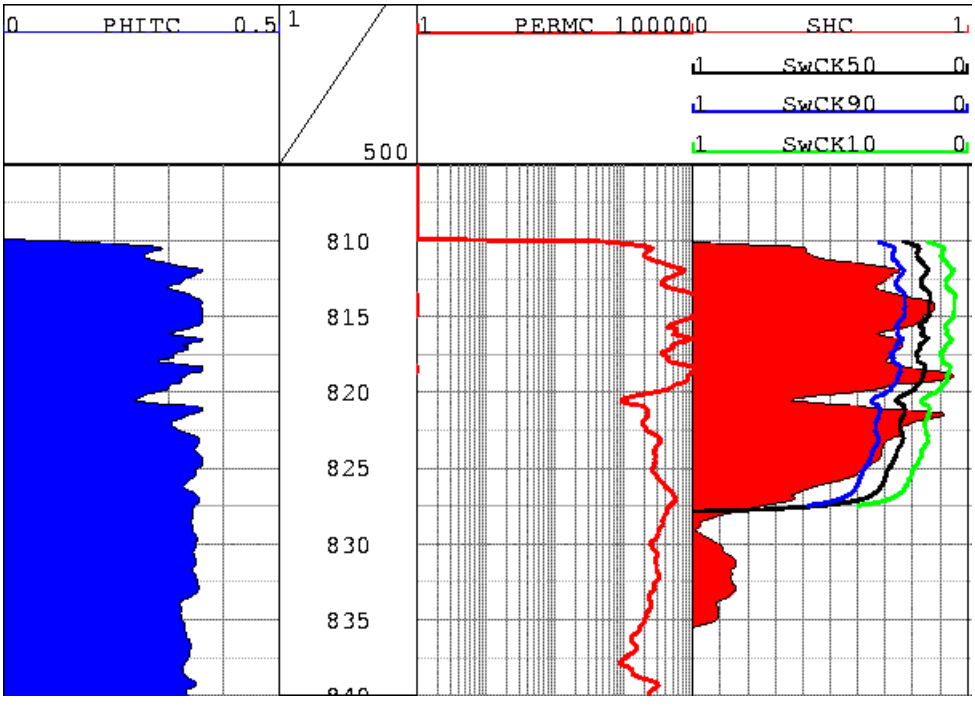

Figure B21a
The porosity (PHITC), permeability (PERMC) & gas saturations (SHC from logs, SWCK50, SWCK90 & SWCK10 are P50, P90 & P10 Sw values from perm based cap. curves using FWL at 827.9 m RT, 818.1 mss) for Sole-1.

In Sole-2, the match between log-derived water saturations and those from the saturation-height functions derived in §2 is reasonable. Although the saturation-height functions suggest a sharper transition zone should be present, §5.4.1 explains why this is not observed. In any case, the range of the gas saturations covered by the saturation-height functions is close to matching the log derived gas saturations over the entire gas column.

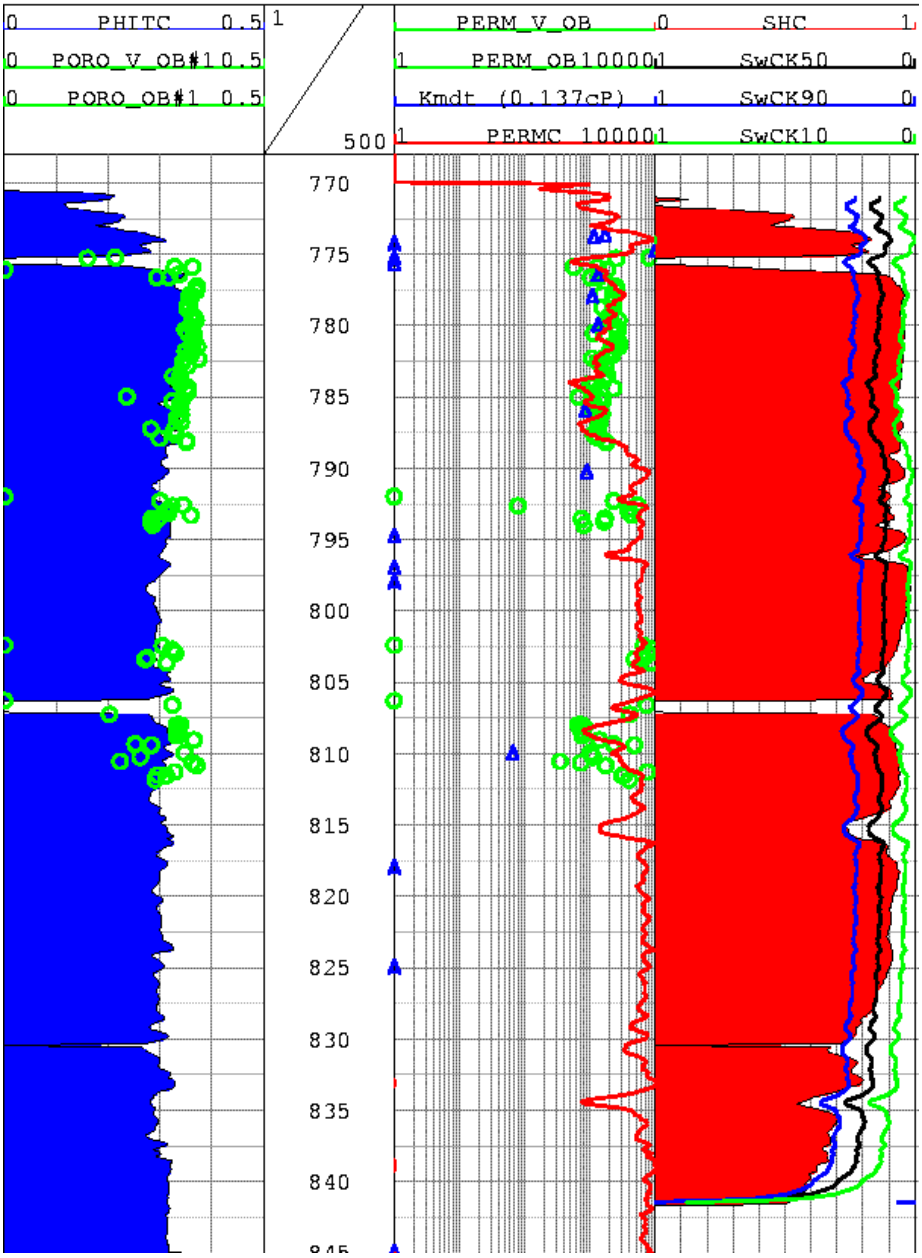

Figure B21b *The evaluated porosities (PHITC from log, PORO_OB & PORO_V_OB from core), permeabilities (PERMC from log, PERM_OB & PERM_V_OB from core, Kmdt from MDT formation pressure tester log) and gas saturations (SHC from logs, SWCK50, SWCK90 & SWCK10 are P50, P90 & P10 gas saturations from permeability based saturation-height functions using a FWL at 816.6 mss) are compared with each other for Sole-2.*

Figure B22a Compares the differences between the logs and the modelled saturations more directly for Sole-1 and Sole-2. The areas where the saturation-height function gives higher gas saturations than the logs (above the diagonal line) are indicative of the transitions zones and the poorly resolved gas saturations at the crest of Sole-1.

Figure B22b Is a histogram of the differences, showing a strongly bimodal distribution. The right-most peak corresponds to the interval above the transition zone in Sole-2 where the log-derived gas saturations average slightly higher than the saturation-height functions. On average the log derived gas saturations are 2 saturation units less than the saturation-height functions. The left-most peak contains data from both Sole-1 and Sole-2, corresponding to the transition zones in both wells and the poorly resolved gas saturations at the crest of Sole-1.

Statistical analysis of the differences between the log and saturation-height derived gas saturations gives an uncertainty at the P90/P10 levels of ±0.17 when all the data is considered. If Sole-2 is considered on its own and the transition zone data removed, the mean difference between the log and saturation-height function is +0.05 saturation units with uncertainty at the P90/P10 levels of ±0.06. Given the data available, this match is considered reasonable i.e. the saturation-height functions can be used to model water saturations for scenario modelling.

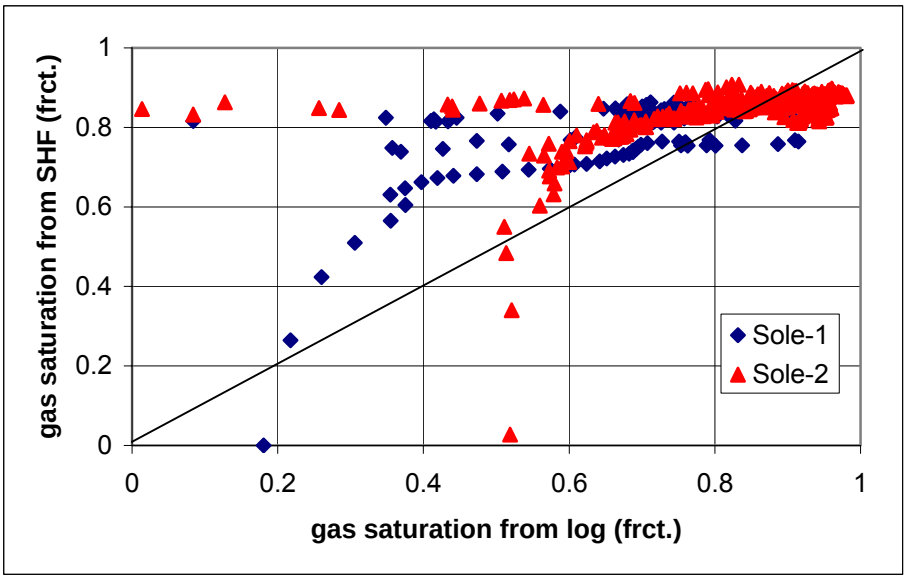

Figure B22a *Comparison between the log and saturation-height derived gas saturations in Sole-1 and Sole-2.*

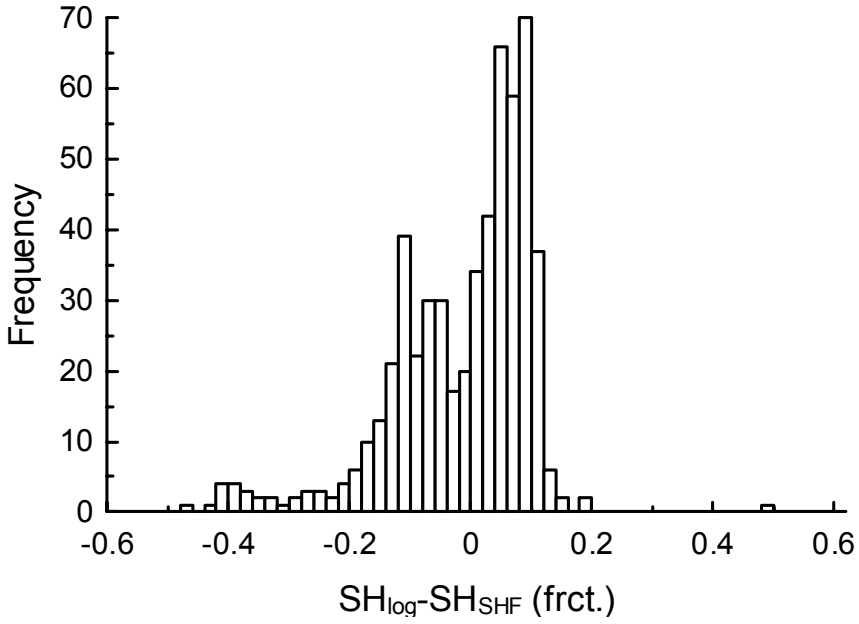

Figure B22b *Histogram of the differences between the log and saturation-height derived gas saturations for the gas column above the transition zones in Sole-1 and Sole-2.*

5.5 Representative Sampling

A cross-check has been made to determine whether the logs, routine and special core analysis work have sampled similar proportions of reservoir quality. Figure B23a displays a normalised histogram of the log porosity (from Sole-1 and 2 above the FWL), routine core porosities and the samples used for capillary pressure work. Figure B23b shows the permeability distributions for the same groups.

It is interesting to note that the *Figures* suggest the core has under-sampled the poorer porosities (less than 30%) and the higher permeabilities (greater than 10 $^{3.6}$ ≈4000 mD). This apparent conflict is readily explained: The core has under-sampled the best facies in the reservoir i.e. those sands with porosities near 30% but permeabilities exceeding 4000 mD. These are the lower gamma ray Facies.

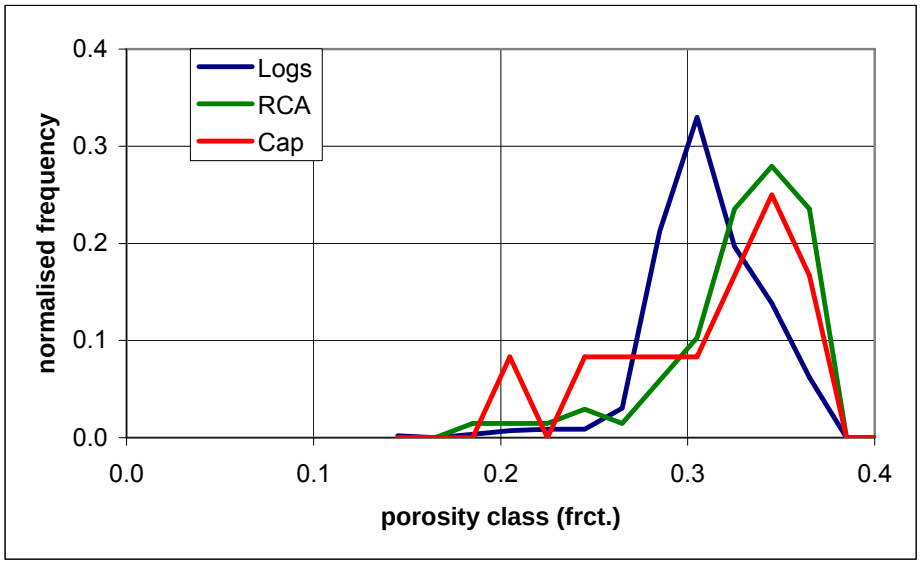

Figure B23a
A normalised histogram of the log porosity (from Sole-1 & 2 above the FWL), routine core porosities and the samples used for capillary pressure work.

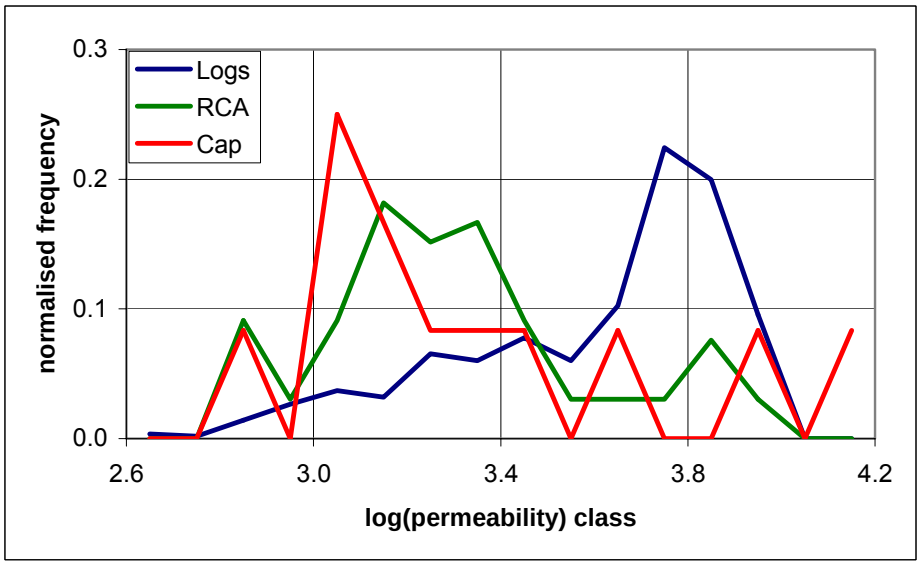

Figure B23b
A normalised histogram of the log derived log10(permeability) (from Sole-1 & 2 above the FWL), routine core log10(permeability) and the samples used for capillary pressure work.

5.6 Formation Water Salinity

None of the documentation available contains any information related to formation water sampling, so there are no direct measurements of formation water salinity.

Indirect estimates of formation water salinity have been made here by looking at the apparent formation resistivity of the water-bearing Latrobe sands. Details for Sole-2 are given in §3.6, results from the other wells are discussed in this section. Figure B24a displays the apparent formation water salinities calculated for the Latrobe Formation in the study wells. Note that in Leatherjacket-1, there are no fully water-bearing sections of reasonable reservoir in the Latrobe Formation, so the shales to either side of the reservoir sections have been used to determine formation water salinity near 15,000 ppm NaCl eq. Hammerhead-1 will be discussed separately.

Also shown on Figure B24a are the range of water salinities used for this field study. Looking at the area circled in black, there appears to be slightly fresher water present than in the deeper section below. For the Sole Field, the depths near the FWL (i.e. the circled zone) appear to be well modelled by the salinities used. Figure B24b shows a histogram of the apparent water salinities in this circled area. The results are the same as reported for Sole-2 alone in §3.6.

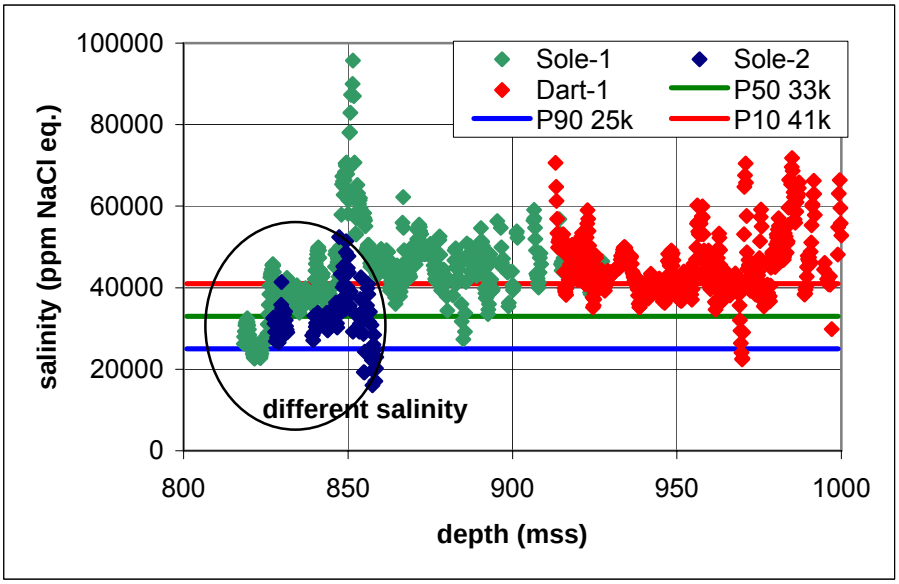

Figure B24a
Estimates of formation water salinity through the water-bearing Latrobe are compared for Sole-1, Sole-2 and Dart-1.

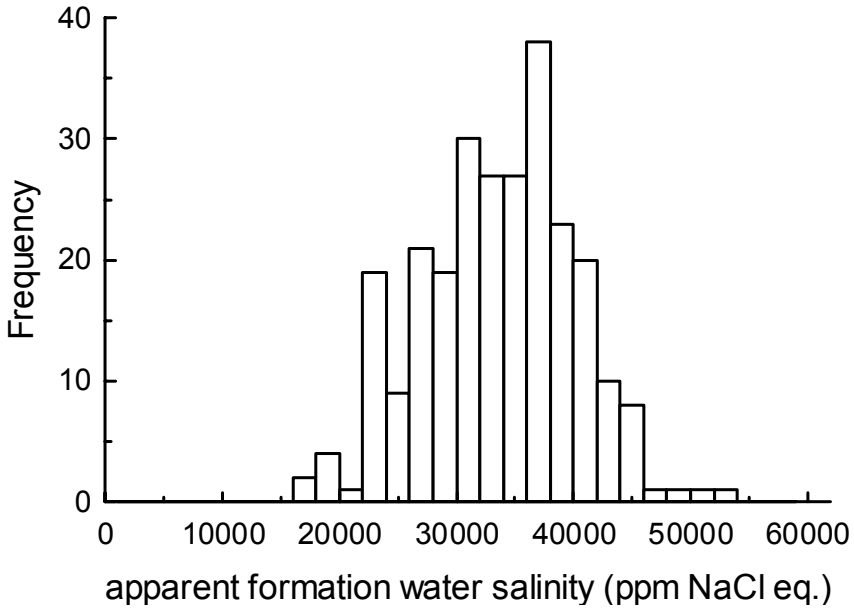

Figure B24b
Histogram of apparent formation water salinity for the zones near the FWL in Sole-1 & Sole-2. The mean is 33,000 ppm NaCl eq., while the uncertainty at the P10/P90 level is ±8000 ppm NaCl eq.

Slightly more saline waters are present below the highlighted zone. Figure B24c is a histogram of this data (i.e. excluding the black circle in Figure B24a). The mean of this data is 44,000 ppm NaCl eq., with uncertainty at the P90/P10 levels of ±7000 ppm NaCl eq. When to use this salinity must be considered in a regional context, as is discussed below.

For completeness, Figure B24d is a combined histogram showing the apparent formation water salinity for the Latrobe Formation in both Sole wells below the FWL and in Dart-1.

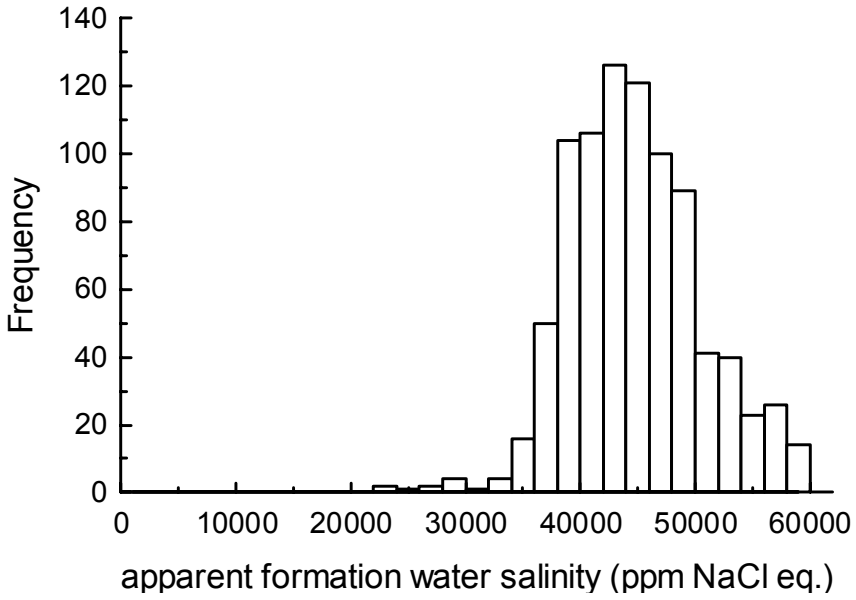

Figure B24c
Histogram of apparent formation water salinity for the zones well below the FWL in Sole-1 & Dart-1. The mean is 44,000 ppm NaCl eq., while the uncertainty at the P10/P90 level is ±7000 ppm NaCl eq.

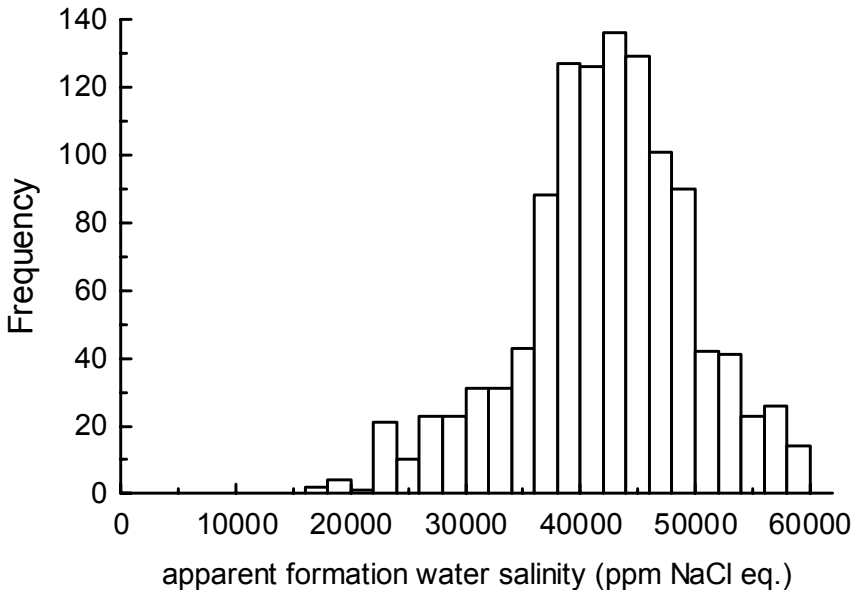

Figure B24d
Histogram of apparent formation water salinity for all zones in Sole-1, 2 & Dart-1.

Looking further afield regionally, Hammerhead-1 data is shown in Figure B24e, along with the other Sole area salinities. A gradual decrease in salinity with depth is apparent, with values near 20,000 ppm NaCl eq. valid for depths below around 1700 mss. Near 1300 mss, values are similar to those recommended for Sole i.e. around 35,000 ppm NaCl eq.

As a guide, using the data provided, it is suggested that the shallower Latrobe intervals may be more subject to salt water influence, having higher salinities than the Latrobe when found at depth.

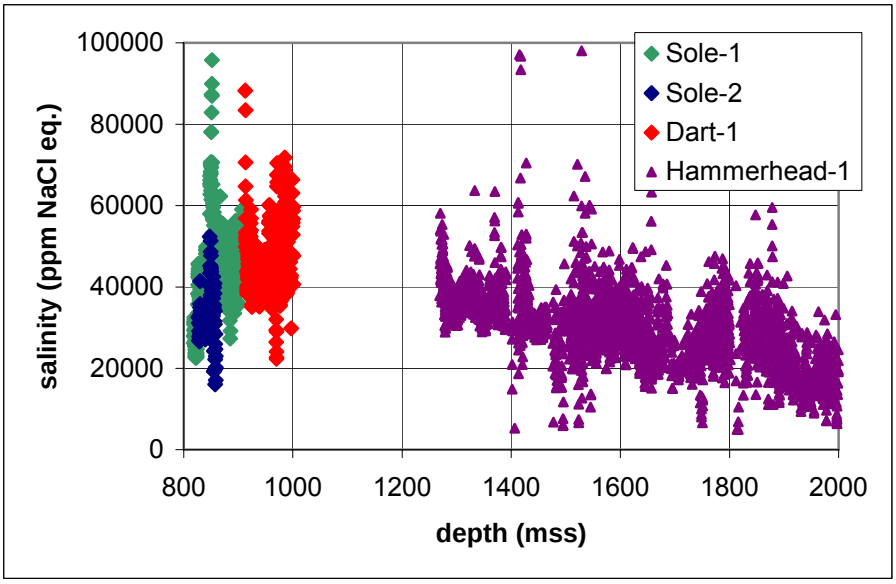

Figure B24e
Estimates of formation water salinity through the water-bearing Latrobe are compared for Sole-1, Sole-2 Dart-1 and Hammerhead-1.

5.7 Pressure Regimes

All the available pressure data for the area has been combined and is displayed in Figure B25a and B25b.

The original water line (1.443 psi/m) can be seen from the Leatherjacket-1 data, being approximately 40 psi above the water line measured in Sole-2. Aquifer depletion owing to production elsewhere in the area explains the pressure decline.

Using the same gas gradient for Sole-1 as that determined in Sole-2 (0.085 psi/m based on the gas composition), a FWL near 819.0 mss is determined. This depth is actually deeper than the 816.6 mss seen in Sole-2 in 2002. Combining this observation with the logged GWC in Sole-1 at 818.1 mss, it seems most likely that the Sole-1 depths are in error. Given that the 40 psi aquifer depletion should have resulted in expansion of the Sole gas column approximately 1 m downward, it can be concluded that the Sole-1 depths are too deep, when compared to Sole-2. A detailed review of the FWL uncertainty has been carried out by Corless (2003), concluding that the most likely absolute depth of the FWL is 817.0 mss. This conclusion matches the observations made in this report.

Note that from the capillary pressure data (§2.9), the difference between the GWC and FWL is consistently less than 0.1 m.

Figure B25a ***All the available formation pressure data for the Sole Field area. The Sole-2 pressure data imply a FWL near 816.6 mss.***

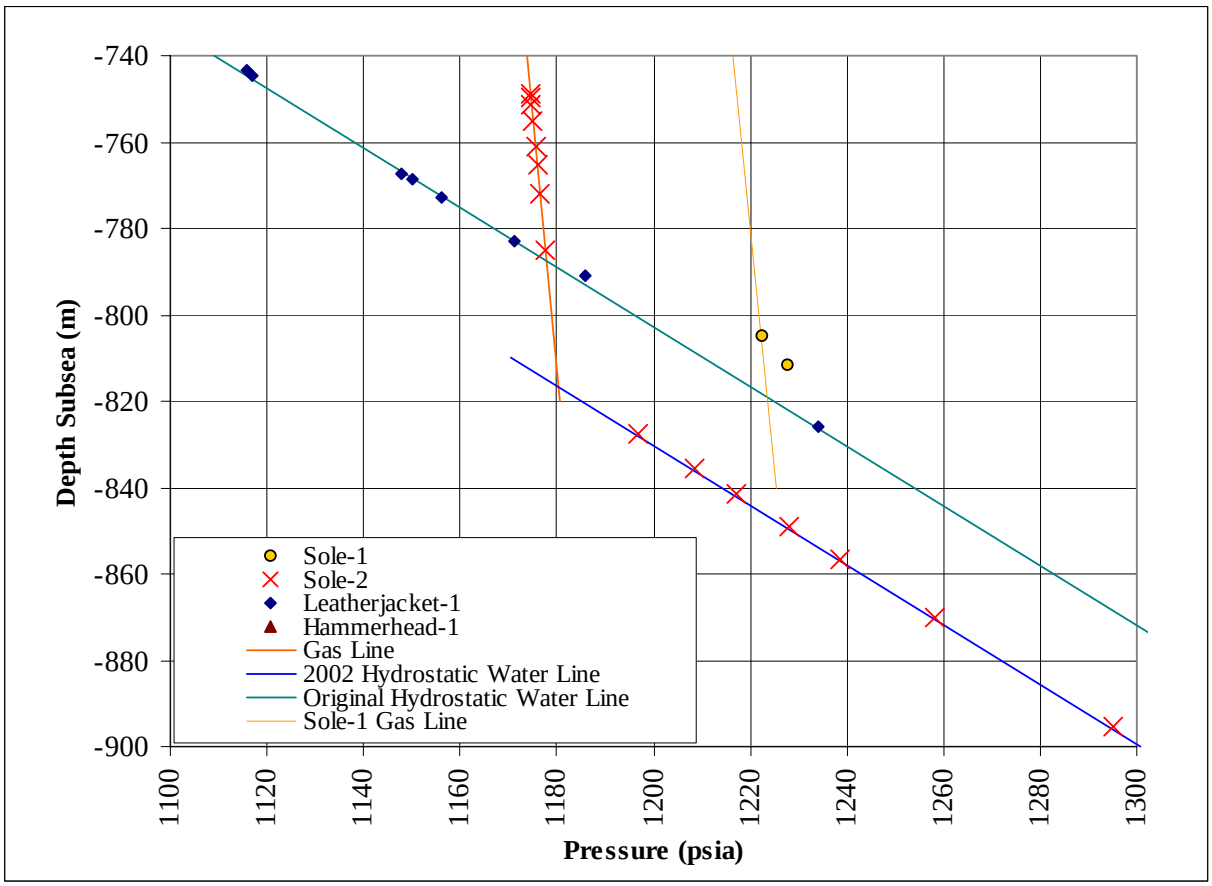

Figure B25b ***All the pressure data for the area is displayed. All the water data from Leatherjacket-1 and Hammerhead-1 lines on the same hydrostatic gradient.***

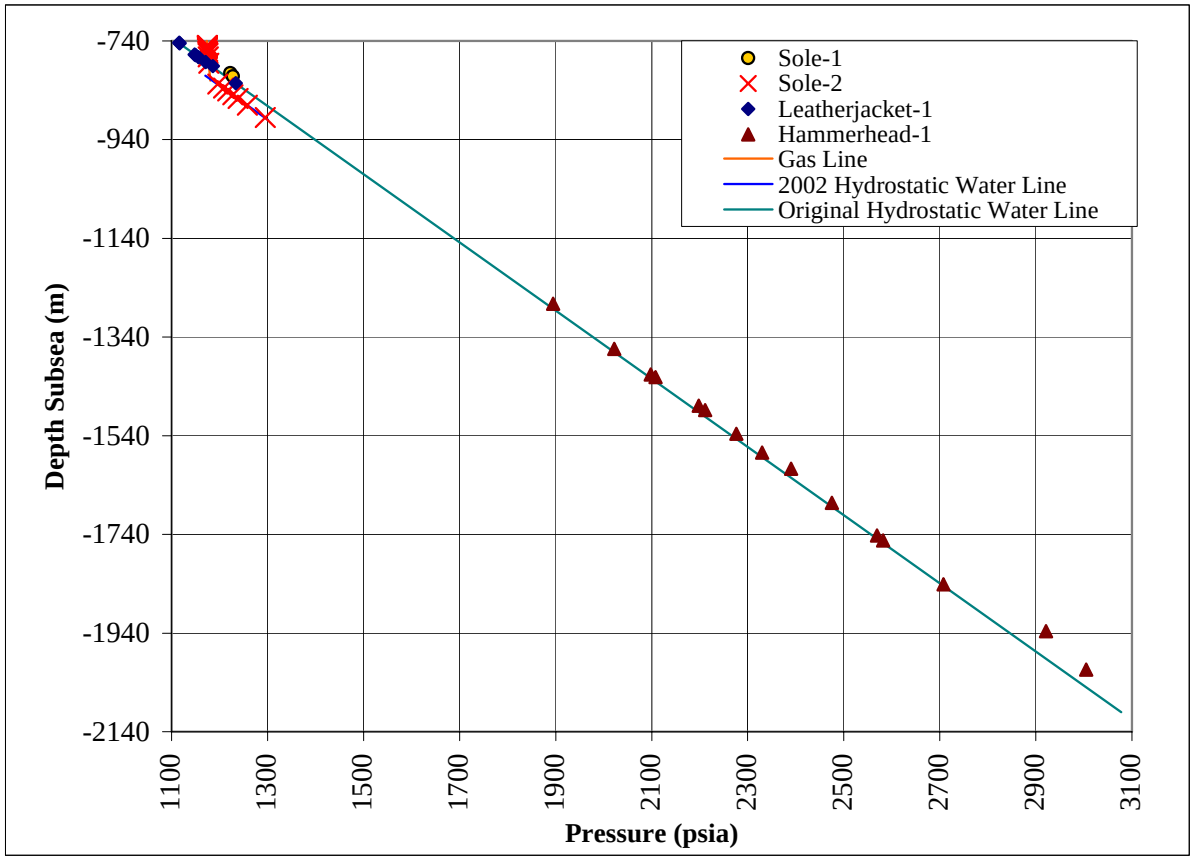

5.8 Reservoir Quality and Water Saturation

Figure B26a shows the porosity plotted against water saturation for the hydrocarbon-bearing Latrobe Formation in the wells studied. Figure B26b shows the gas saturations plotted against permeability instead of porosity. Both figures show two crude trends; hydrocarbon saturations increasing with increasing porosity or permeability (red lines).

There are some anomalies in Sole-2, with some gas saturations showing little variation with permeability (blue oval). It is likely that this is a result of two factors:

i) Imperfections in the permeability modelling, and

ii) Bed resolution differences between the resistivity (gas saturations) and the permeability logs (porosity and GR based).

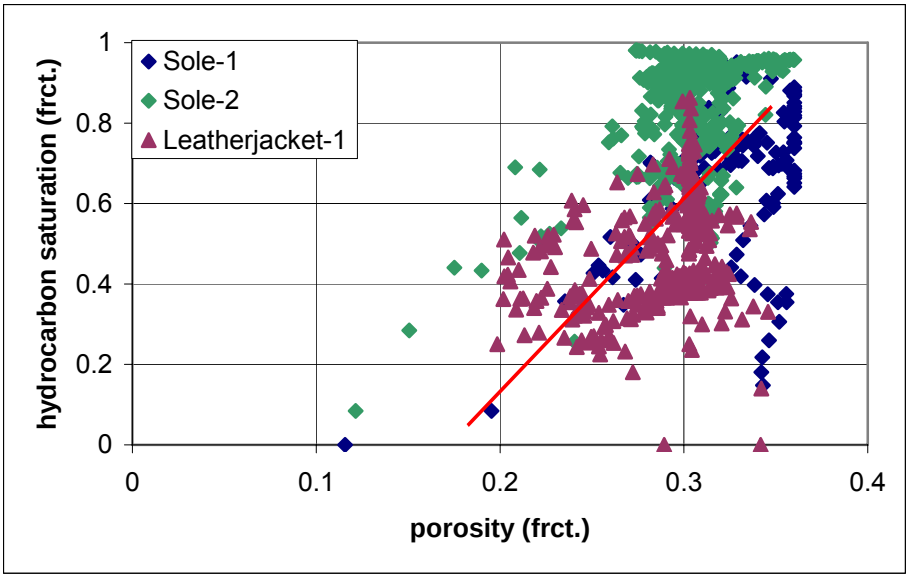

Figure B26a *Hydrocarbon saturation plotted as a function of porosity for Sole-1, 2 & Leatherjacket-1.*

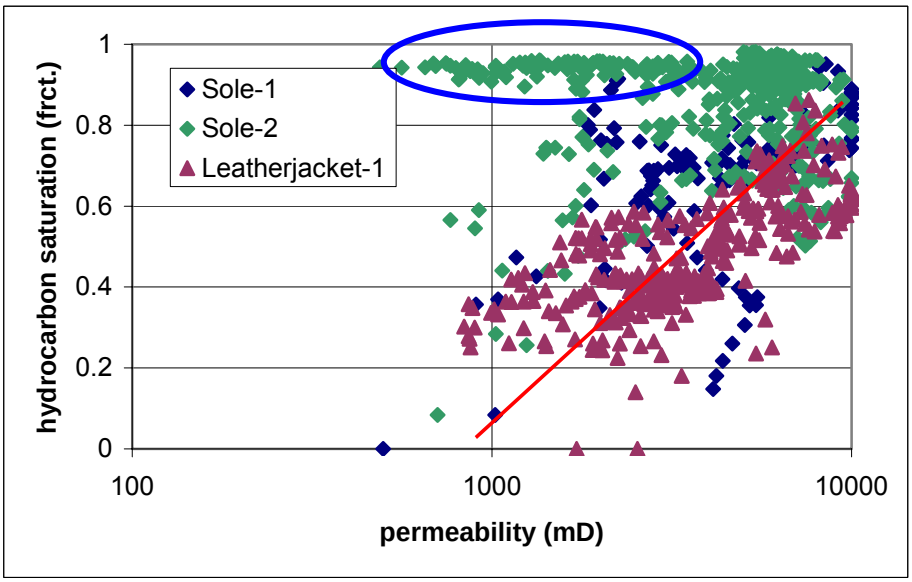

Figure B26b *Hydrocarbon saturation plotted as a function of permeability for Sole-1, 2 & Leatherjacket-1.*

5.9 Uncertainty

To illustrate which factors contribute most to the uncertainties in porosities and hydrocarbon saturations for the Sole Field, the following “Tornado” plots have been constructed using Monte-Carlo modelling. Items toward the tops of the Figures B27a and B27b show the largest impacts on the range of porosities and saturations estimated. Tables B4a and B4b detail the input parameters for the Monte-Carlo analyses.

When the uncertainties are considered simultaneously, uncertainty values for use in volumetric calculations at the P10/P90 levels can be derived. These have been summarised below:

porosity ± 0.015 (or ± 1.5% of bulk volume),

water saturation ± 0.04 (or ± 4% of pore volume).

Additional core information together with good hole conditions for wireline logging in the future presents is the best way of reducing the porosity uncertainty. Reduced porosity uncertainty would also reduce the water saturation uncertainty through both porosity directly and the clay conductivity being estimated.

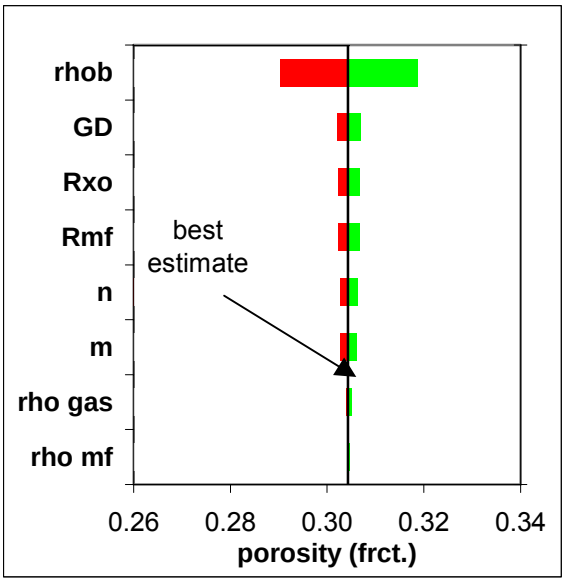

Figure B27a *– Uncertainty ranking for each component contributing to density porosity calculation. Total uncertainty in porosity at the P90/P10 levels is ± 0.015 p.u.*

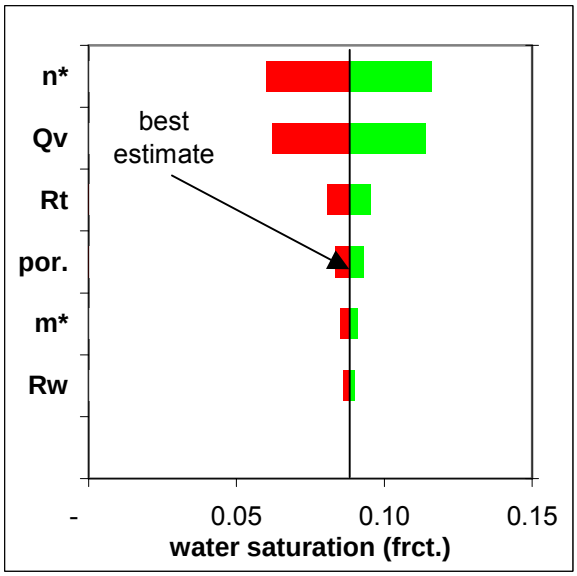

Figure B27b *– Uncertainty ranking for each component contributing to hydrocarbon saturation calculation. Total uncertainty in hydrocarbon saturations at the P90/P10 levels is ± 0.04 s.u.*

Table B4a ***Input parameters for Monte-Carlo modelling of density porosities.***

Parameter	P90	P50	P10	Porosity Uncertainty
rhob	1.955	1.915	1.875	0.0142
GD	2.620	2.647	2.657	0.0025
Rxo	1.800	2.000	2.200	0.0022
Rmf	0.110	0.100	0.090	0.0023
n	2.090	1.930	1.770	0.0019
m	1.810	1.740	1.670	0.0017
rho gas	0.050	0.060	0.070	0.0006
rho mf	1.000	1.010	1.020	0.0001
TOTAL				*0.015*

Table B4b ***Input parameters for Monte-Carlo modelling of gas saturations.***

Parameter	P90	P50	P10	Sw Uncertainty
n*	1.990	2.190	2.390	0.028
Qv	0.092	0.215	0.337	0.026
Rt	69.680	80.000	90.320	0.008
por.	0.290	0.305	0.319	0.005
m*	1.800	1.850	1.900	0.003
Rw	0.161	0.138	0.115	0.002
TOTAL				*0.040*

6 CONCLUSIONS

The study objectives have been met.

- Sole-2 core data has been used to construct: ambient to in-situ porosity and permeability transforms, porosity to permeability transforms, cementation and saturation exponents, saturation-height functions, residual gas saturation relations and in-situ fluid permeabilities.
- For the Sole Gas Field, porosities should be calculated based on the density log with a gas correction using the invaded zone resistivity log to correct for the fluid density in the invaded zone.
- In Sole-2, differences between core and log porosities in the washed out hole section are thought to be due to excess mud invasion into the permeable sands causing increased density measurements. A correction has been applied to the density porosities to improve the match with the core data. The uncertainty addressed by such a model has been quantified.
- In Sole-2, permeabilities estimated from logs compare reasonably with those measured on core. The technique requires normalisation of the gamma ray log in other wells to match that in Sole-2 over selected intervals for application in other Upper Latrobe penetrations. Significant uncertainty in absolute permeability values remains.
- Formation water salinity in the Upper Latrobe Sands of the Sole Field is thought to be in the range from 26,000 to 40,000 ppm NaCl equivalent. Use of 33,000 ppm NaCl eq. for petrophysical evaluation is recommended.
- Gas saturations from capillary pressure based saturation-height functions compare well with log derived water saturations, although there are some differences in the transition zones of Sole-1 and Sole-2. These are thought to be due to limitations of the resistivity readings through these zones in each well.
- The FWL is located near 816.6 mss from Sole-2. Sole-1 gives a deeper GWC near 818.1 mss. However, the FWL is thought to be the same in both wells at a most likely depth near 817.0 mss.

7 RECOMMENDATIONS

The largest uncertainties in the Petrophysical evaluation of the Sole Field lie in the evaluation of Sole-2:

i) The porosity uncertainty in the enlarged hole sections has been addressed here by direct calibration to core porosities. The recommended route is to use grain density and the density log response. Unfortunately in the enlarged sections of Sole-2, the density log readings appear to be reading too high as a consequence of mud solid invasion. Any future wells require special effort to ensure gauge hole and low mud invasion to enable quantitative log evaluation. If there had been no core acquired in Sole-2, the porosity underestimation would not have been so clearly apparent.

ii) The GWC on the conventional logs in Sole-2 appears to be as deep as 848 m RT (823 mss), yet the pressure data is conclusive with the FWL near 841.6 m RT (816.6 mss). Only when the veracity of the laterolog measurements over the extreme washouts is questioned does it become possible to make a coherent story. To fully verify the effect of the washed out hole on the laterolog readings, some electromagnetic modelling of the Sole-2 borehole could be requested from Schlumberger.

Any future Sole development wells will require only the following basic logging suite, provided work can be done to ensure optimal hole conditions. Note that the logs marked in red are the most important for quantitative Petrophysical evaluation. These logs require the most effort to optimise their measurement accuracy. The logs marked in blue are the least important:

Gamma Ray/Caliper/Density/Neutron/Sonic/Deep & Shallow Resistivity/Invaded Zone Resistivity

8 REFERENCES

Adams, S.J., Farmer, R.G. Hawton, D. and Seybold, O.: "Laboratory and In-Situ Determination of Residual Gas Saturations in Maui," proceedings of N.Z. Petroleum Conference, Christchurch, 19-23 March 2000.

Baker, J.C.: “Petrology, Diagenesis and Reservoir Quality of Samples from Sole-2,” Reservoir Solutions Pty. Ltd. Report for OMV Australia Pty. Ltd., 6 January 2003.

Choo, C.: “Discrepancy Between Log Derived and Capillary Pressure Derived Oil Saturations in the Transition Zone of Wanaea-1,” FESWA Formation Evaluation Seminar, Perth, Australia, 6 December 1991.

Juhasz, I.: "Assessment of the distribution of shale, porosity and hydrocarbon saturation in shaley sands," paper AA, Chapter 15, in 10th European Formation Evaluation Symposium transactions, SPWLA, Aberdeen, 1986.

Land, C.S.: “Calculation of Imbibition Relative Permeability for Two- and Three-Phase Flow from Rock Properties,” SPE 1942, Transactions Volume 243, June 1968.

Nieto, J.A., Yale, D.P., and Evans, R.J.: “Improved methods for correcting core porosity to reservoir conditions,” The Log Analyst, v. 35, no. 3, p. 21-30, 1994.

Waxman, M.H., and Smits, L.J.M.; "Electrical conductivities in oil-bearing shaly sands," Society of Petroleum Engineers Journal, v. 8(2), p. 107-122, 1968.

APPENDIX BA – SATURATION-HEIGHT IMPLEMENTATION

To utilise the drainage functions provided below, it is necessary to know the porosity (f) or permeability (k) of the piece of reservoir being modelled and the height (h) of the reservoir piece above the original Free-Water Level (FWL) i.e. the FWL at the time hydrocarbons were emplaced in that piece of rock. Note that the porosity-based saturation-height functions presented do not work as well as the permeability-based equations.

Appendix BA.1 Porosity Based Drainage Function

For the Sole Field, drainage porosity-based saturation-height functions are Thomeer in form i.e. calculate the following curve (SwD):

S_{wD} = 1 - a·exp(-G/log10(h/h_d)),

Where a = 1.032,

G = 0.424,

h_d = 0.190 ,

h_o = (FWL – (true vertical depth below mean sea level of point in reservoir)) in metres

FWL is Free Water Level in true vertical depth below mean sea level in metres

This formula is only valid for porosities in the range 10 to 40% and for heights between zero and 80 m above the FWL. In addition, any values of S_{wD} falling outside the range 0.01 to 1.0 should be set to 1.0. Note that the uncertainty in water saturations estimated using this relationship is ±0.116 at the P90/P10 levels.

Appendix BA.2 Permeability Based Drainage Function (No Facies)

For the Sole Field, drainage permeability-based saturation-height functions are also Thomeer in form i.e. calculate the following curve (SwD):

S_{wD} = 1 - a·exp(-G/log10(h/10 ^{hd})),

where a = a_1· log10(k) +a_2,

G = l_1· log10(k) +l_2,

h_d = h_1· log10(k) +h_2,

a_1, a_2, l_1, l_2, h_1, h_2 in *Appendix Table B1*, below,

k = stressed and Klinkenberg corrected permeability in milliDarcies

h_o = (FWL – (true vertical depth below mean sea level of point in reservoir)) in metres

FWL is Free Water Level in true vertical depth below mean sea level in metres

This formula is only valid for permeabilities in the range 100 to 20000 mD and for heights between zero and 80 m above the FWL. In addition, any values of S_{wD} falling outside the range 0.01 to 1.0 should be set to 1.0.

Note that the uncertainties in these estimates at the P10 and P90 levels are given in the following table i.e. at the P10 level S_w = S_{wD}-PI, while at the P90 level S_w = S_{wD}+PI.

Appendix Table BA1- Drainage permeability-based Thomeer function parameters for the Sole Field.

a_1	a_2	l_1	l_2	h_1	h_2	PI
0.059	0.851	-0.005	0.481	-0.35	0.394	0.094

Appendix BA.3 Permeability Based Drainage Function (Facies Based)

For the Sole Field, drainage permeability-based saturation-height functions are also Thomeer in form i.e. calculate the following curve (SwD):

S_{wD} $= a\cdot(h - h_d)^{-\lambda}$,

where $a = a_1 \cdot \log10(k) + a_2$,

$\lambda = l_1 \cdot \log10(k) + l_2$,

$h_d = h_1 \cdot \log10(k) + h_2$,

$a_1, a_2, l_1, l_2, h_1, h_2$ in *Appendix Table B2*, below,

k = stressed and Klinkenberg corrected permeability in milliDarcies

h_o = (FWL – (true vertical depth below mean sea level of point in reservoir)) in metres

FWL is Free Water Level in true vertical depth below mean sea level in metres

This formula is only valid for permeabilities in the range 100 to 20000 mD and for heights between zero and 80 m above the FWL. In addition, any values of S_{wD} falling outside the range 0.01 to 1.0 should be set to 1.0.

Note that the uncertainties in these estimates at the P10 and P90 levels are given in the following table i.e. at the P10 level $S_w = S_{wD}$-PI, while at the P90 level $S_w = S_{wD}$+PI.

Appendix Table BA2- Drainage permeability-based Thomeer function parameters for the Sole Field, using GR to define the Facies.

Facies	a_1	a_2	l_1	l_2	h_1	h_2	PI
GR>86	-0.489	1.916	-0.040	0.390	0.420	-0.939	0.085
GR<86	-0.174	0.996	0.087	0.003	0.039	0.082	0.096

APPENDIX BB.1 – AVAILABLE LOGS FOR SOLE FIELD STUDY

Well	Log Type	From (m RT)	To (m RT)	Remarks
Sole-1	CALI	290	1128	Caliper log.
	DRHO	138	1128	Density correction log.
	DT	290	1128	Sonic log.
	GR	138	1128	Gamma ray.
	ILD	290	1128	Deep resistivity log.
	MLL	290	1128	Invaded zone resistivity log.
	NPHI	665	1128	Neutron log.
	RHOB	290	1128	Density log.
	SN	290	1128	Short normal resistivity.
	SP	290	1128	Spontaneous potential.
Sole-2	BS	650	1000	Bit size.
	DT4P	650	1000	Compressional sonic log.
	EHGR	650	1000	Gamma ray.
	HCAL	650	1000	Caliper log.
	HDRA	650	1000	Pseudo density correction log.
	HLLD	650	1000	Deep resistivity log.
	HLLS	650	1000	Shallow resistivity.
	HTHO	650	1000	Spectral Gamma Ray - Thorium.
	HURA	650	1000	Spectral Gamma Ray - Uranium.
	PEFZ	650	1000	Photoelectric Effect.
	RHOZ	650	1000	Density log.
	RXOZ	650	1000	Invaded zone resistivity log.
	SP	650	1000	Spontaneous potential.
	TNPH	650	1000	Neutron log.
Dart-1	CALI	595	1218	Caliper log.
	DRHO	793	1218	Density correction log.
	DT	252	1218	Compressional sonic log.
	GR	123	1218	Gamma ray.
	ILD	600	1218	Deep resistivity log.
	NPHI	793	1218	Neutron log.
	RHOB	793	1218	Density log.
	SFL	600	1218	Shallow resistivity.
	SP	595	1218	Spontaneous potential.
Hammer-head-1	CALI	525	2108	Caliper log.
	DT	1184	2108	Compressional sonic log.
	GR	525	2108	Gamma ray.
	ILD	556	1037	Deep induction resistivity log.
	LLD	1184	2108	Deep laterolog resistivity log.
	LLS	1184	2108	Shallow laterolog resistivity log.
	MSFL	1184	2108	Invaded zone resistivity log.
	NPHI	525	2108	Neutron log.
	RHOB	525	2108	Density log.
	SFL	556	1196	Shallow resistivity.

Leather-jacket-1	CALI	630	930	Caliper log from resistivity run.
	CALS	630	930	Caliper log from sonic run.
	CNL	630	932	Neutron log.
	DRHO	630	940	Density correction log.
	DTL	630	924	Compressional sonic log – long-spaced.
	GR	100	928	Gamma ray.
	LLD	630	945	Deep laterolog resistivity log.
	LLS	630	945	Shallow laterolog resistivity log.
	MSFL	630	934	Invaded zone resistivity log.
	PEFZ	630	940	Photoelectric Effect.
	RHOB	630	940	Density log.
	SP	630	912	Spontaneous potential.

APPENDIX BB.2 – LOG NAME CONVENTION FOR SOLE FIELD STUDY

Log Name	Description*	Scale	
		left	***right***
CALI	resistivity caliper (inches)	6-8	16-18
DRHO	density correction log (g/cc)	-0.75	0.25
DT	sonic log (μs/ft)	140	40
DT4P	PEX sonic log (μs/ft)	140	40
GR	gamma ray (API)	0	150
HCAL	caliper (inches)	6-8	16-18
HDRA	pseudo-density correction log (g/cc)	-0.75	0.25
HLLD	deep laterolog resistivity (ohm.m)	0.2	200
HLLS	shallow laterolog resistivity (ohm.m)	0.2	200
ILD	deep induction resistivity (ohm.m)	0.2	200
MDT	in-situ permeability estimated from MDT (mD)	1	10000.0
MLL	invaded zone resistivity (ohm.m)	0.2	200
NPHI	neutron porosity (frct.BV)	0.45	-0.15
PERM_(V_)OB	in-situ core permeability (mD)	1	10000
PERMC	in-situ permeability (mD)	1	10000.0
PHIRT	total porosity from RT, assuming Sh=0 (frct.BV)	0	0.5
PHITC	total porosity in reservoir = RES*POR (frct.BV)	0	0.5
PHITE	total porosity in reservoir directly calibrated to core (frct.BV)	0	0.5
PORC	total porosity for all rock based on selection from following 3 datasets (frct.BV)	0	0.5
PORDC	density porosity (frct.BV)	0	0.5
PORO_(V_)OB	in-situ core porosity (frct.BV)	0	0.5
PORSC	sonic porosity (frct.BV)	0	0.5
RD	deep resistivity (ohm.m)	0.2	200
RESC	reservoir flag (0=non-reservoir, 1 = reservoir)	0	1
RHOB	density log (g/cc)	1.95	2.95
RHOZ	density log (g/cc)	1.95	2.95
RS	shallow resistivity (ohm.m)	0.2	200
RXOZ	invaded zone resistivity (ohm.m)	0.2	200
SEALC	sealing lithology flag (0=non-seal, 1 = seal)	0	1
SFL	shallow resistivity (ohm.m)	0.2	200
SHC	hydrocarbon saturation (frct.PV)	0	1
SHXOC	invaded zone hydrocarbon saturation (frct.PV)	0	1
SN	short normal resistivity (ohm.m)	0.2	200
SP	spontaneous potential (mV)	0	100
SW(C)K10	P10 Sw from perm based saturation height (frct.PV)	0	1
SW(C)K50	P50 Sw from perm based saturation height (frct.PV)	0	1
SW(C)K90	P90 Sw from perm based saturation height (frct.PV)	0	1
TNPH	PEX neutron porosity (frct.BV)	0.45	-0.15

APPENDIX BC – LOG EVALUATION SUMMARY & PLOTS

Well	Unit	From (m RT)	To (m RT)	From (mss)	To (mss)	Gross	Net	N/G	ϕ	perm	Sh	HCPV	Comment
Sole-2	Gas-Bearing Latrobe	770.0	841.6	745.0	816.6	71.6	69.3	0.97	0.303	3939.4	0.850	17.836	Mobile gas.
Sole-2	Water-Bearing Latrobe	841.6	871.5	816.6	846.5	29.9	29.9	1.00	0.317	2416.9	0.066		Mobile water.
Sole-2	All Latrobe	770.0	871.5	745.0	846.5	101.5	99.2	0.98	0.307	3400.6	0.606		All Latrobe.
Sole-1	Gas-Bearing Latrobe	810.0	827.9	*800.2*	*818.1*	17.9	17.9	1.00	0.326	3978.0	0.663	3.864	Mobile gas.
Sole-1	Water-Bearing Latrobe	827.9	890.0	*818.1*	*880.2*	62.1	62.1	1.00	0.312	2812.7	0.013		Mobile water.
Sole-1	All Latrobe	810.0	890.0	*800.2*	*880.2*	80.0	80.0	1.00	0.315	3040.6	0.164		All Latrobe.
Dart-1	Latrobe	921.0	991.0	911.2	981.2	70.0	69.2	0.99	0.319	4268.2	0.001		Mobile water.
Dart-1	Latrobe	991.0	1123.0	981.2	1113.2	132.0	130.0	0.99	0.255	396.3	0.018		Mobile water.
Dart-1	Golden Beach	1123.0	1212.0	1113.2	1202.2	89.0	2.0	0.02	0.302	2872.0	0.000		Mobile water.
Hammerhead-1	Upper Latrobe	1291.0	1383.2	1269.0	1361.2	92.2	92.2	1.00	0.277	1409.3	0.000		Mobile water.
Hammerhead-1	Lower Latrobe	1391.0	1520.0	1369.0	1498.0	129.0	129.0	1.00	0.227	124.9	0.015		Mobile water.
Hammerhead-1	Lower Latrobe	1528.0	1830.0	1506.0	1808.0	302.0	302.0	1.00	0.159	7.3	0.009		Mobile water.
Hammerhead-1	Golden Beach	1830.0	1948.0	1808.0	1926.0	118.0	72.0	0.61	0.188	24.8	0.016		Mobile water.
Hammerhead-1	Strzelecki	1948.0	2108.0	1926.0	2086.0	160.0	42.2	0.26	0.127	1.9	0.100		Mobile water.
Leatherjacket-1	Latrobe	756.5	762.0	735.5	741.0	5.5	5.2	0.94	0.282	2309.7	0.202		Mobile water.
Leatherjacket-1	Latrobe	763.8	772.7	742.8	751.7	8.9	8.3	0.93	0.303	5514.9	0.596	1.497	Mobile oil.
Leatherjacket-1	Latrobe	774.7	776.5	753.7	755.5	1.8	1.3	0.75	0.303	1934.6	0.522	0.214	Possibly mobile oil.
Leatherjacket-1	Latrobe	778.5	789.0	757.5	768.0	10.5	10.5	1.00	0.302	6641.2	0.531	1.680	Mobile oil.
Leatherjacket-1	Latrobe	789.0	806.8	768.0	785.8	17.8	17.8	1.00	0.296	2951.1	0.307		Mobile water.
Leatherjacket-1	Latrobe	811.1	819.1	790.1	798.1	8.0	8.0	1.00	0.268	3328.0	0.532	1.140	Mobile oil.
Leatherjacket-1	Latrobe	819.1	823.0	798.1	802.0	3.9	3.3	0.85	0.246	2038.7	0.295		Mobile water.
Leatherjacket-1	Latrobe	763.8	789.0	742.8	768.0	25.2	20.2	0.80	0.302	5657.5	0.557	3.399	Mobile oil.

Appendix Table B3 –Petrophysical evaluation summary data for the Sole Study Area Wells. Hydrocarbon saturations from wireline logs.

Appendix BC.1 Sole-1 Log Evaluation

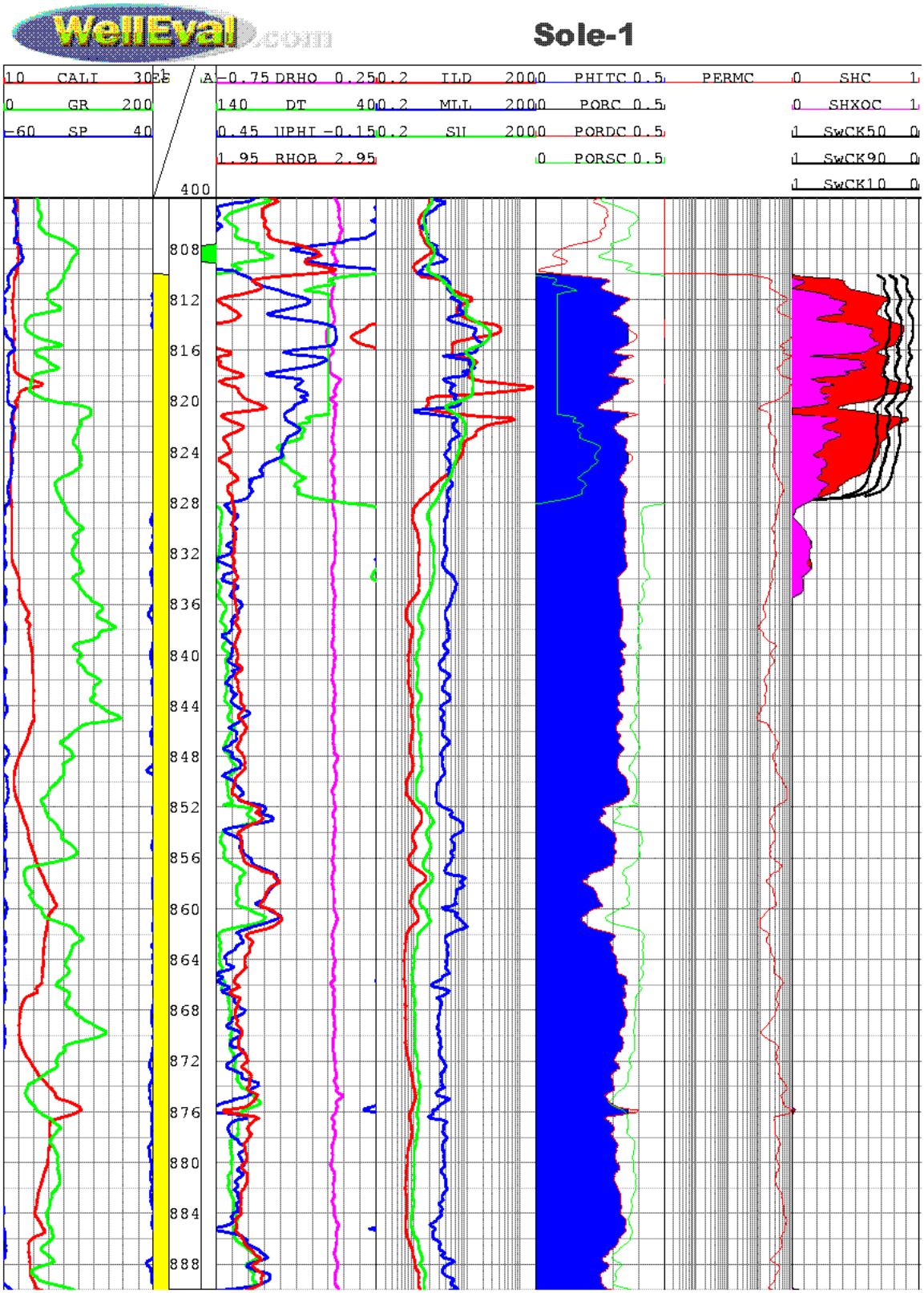

Page 1

Appendix BC.2 Sole -2 Log Evaluation

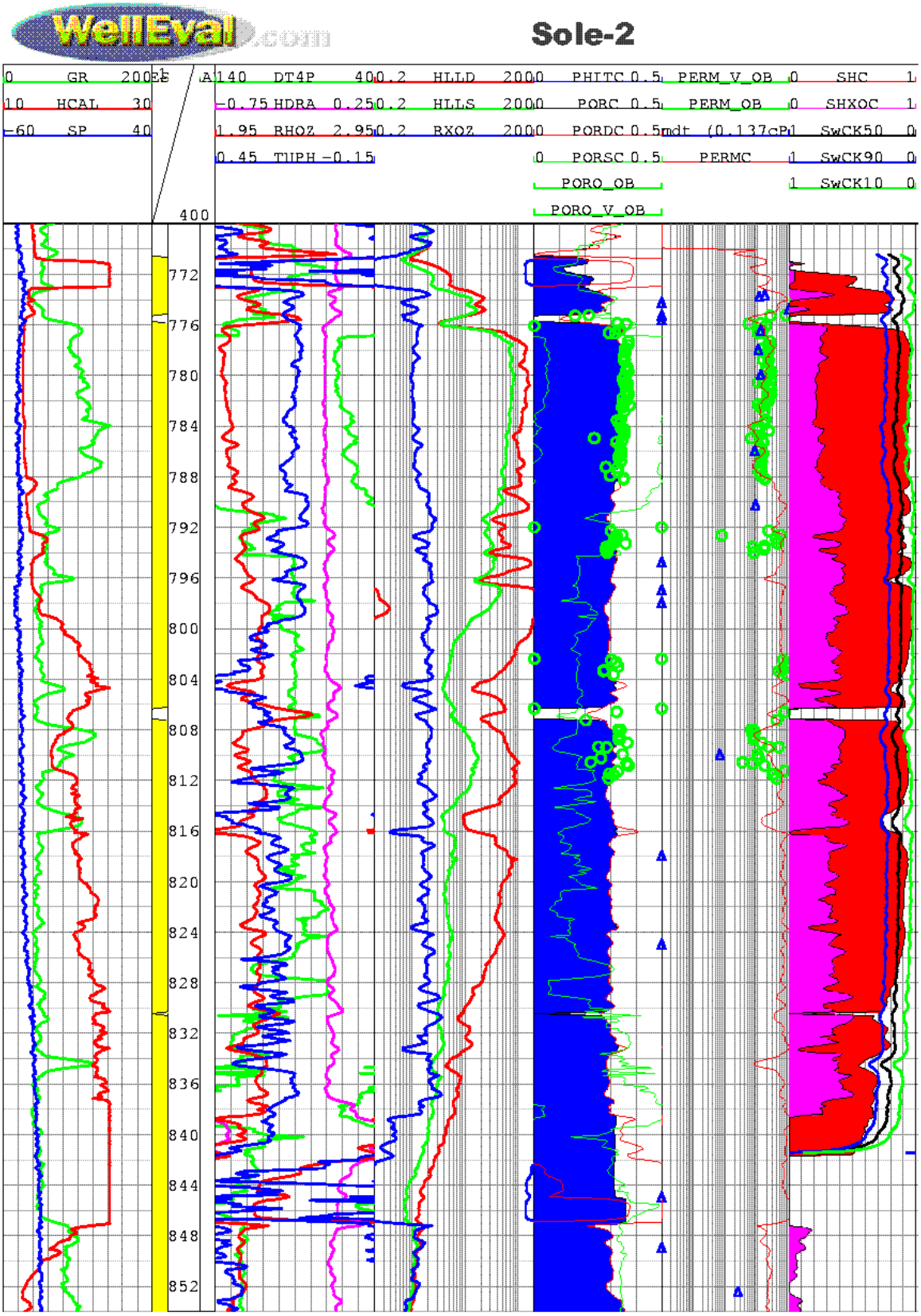

Appendix BC.3 Dart -1 Log Evaluation

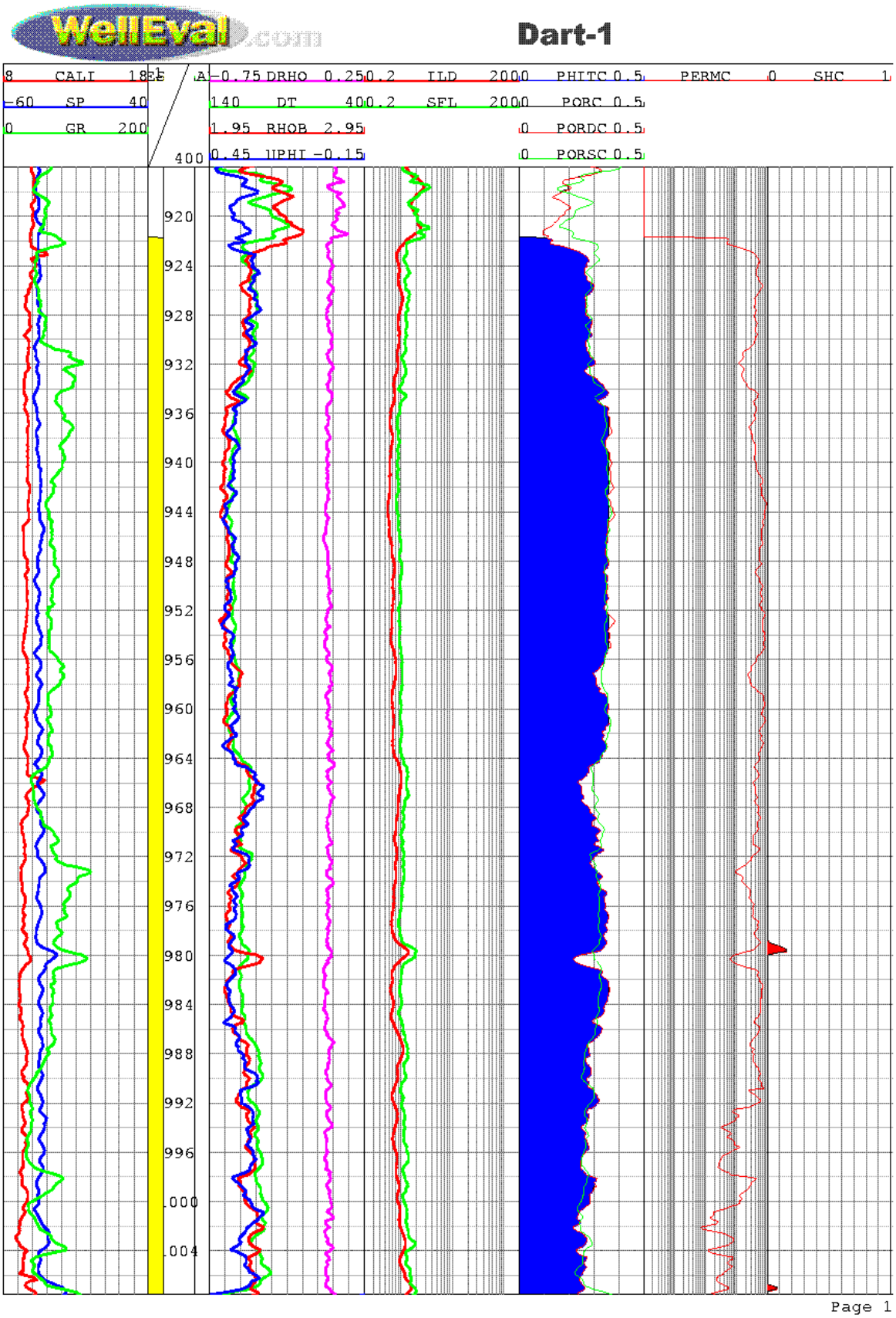

Appendix BC.4 Hammerhead-1 Log Evaluation

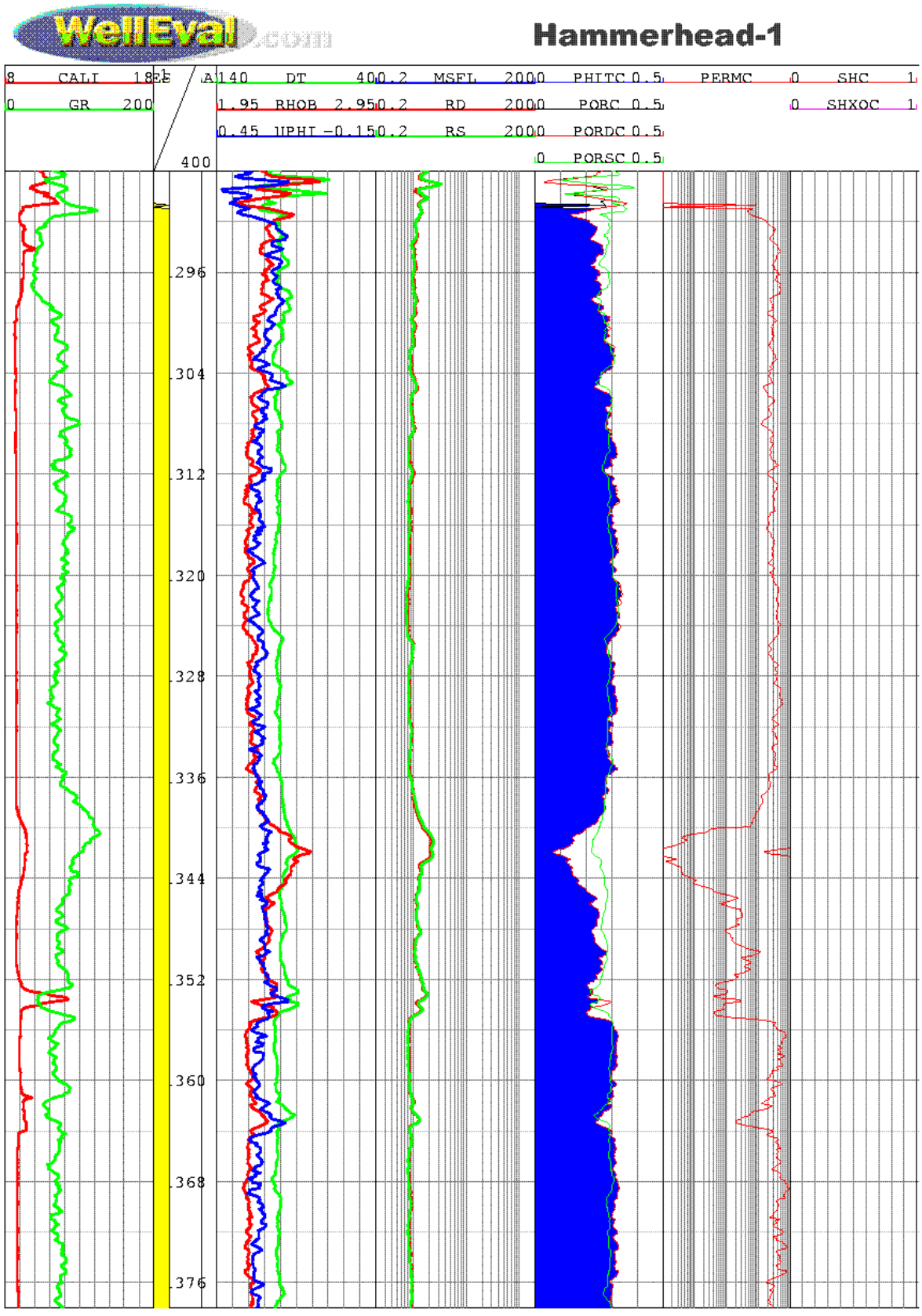

Page 1

Appendix BC.5 Leatherjacket-1 Log Evaluation